Clim. Past Discuss., https://doi.org/10.5194/cp-2018-78
Manuscript under review for journal Clim. Past
Discussion started: 11 July 2018

Climate of the Past Discussions

Deglacial to postglacial history of Nares Strait, Northwest Greenland: a marine perspective

Eleanor Georgiadis[1,2], Jacques Giraudeau[1], Philippe Martinez[1], Patrick Lajeunesse[2], Guillaume St-Onge[3], Sabine Schmidt[1], Guillaume Massé[2]

[1]Université de Bordeaux, CNRS, UMR 5805 EPOC, 33615 Pessac, France
[2]Université Laval, UMI 3376 TAKUVIK, Québec, G1V 0A6, Canada
[3]Université du Québec à Rimouski and GEOTOP Research Center, Institut des sciences de la mer de Rimouski (ISMER), Rimouski, G5L 3A1, Canada

Correspondence to: Eleanor Georgiadis (eleanor.georgiadis@u-bordeaux.fr)

Abstract. A radiocarbon dated marine sediment core retrieved in Kane Basin, central Nares Strait, was analysed to constrain the timing of the postglacial opening of this Arctic gateway and its Holocene evolution. This study is based on a set of sedimentological and geochemical proxies of changing sedimentary processes and sources that translate into ice sheet configuration in the strait. Proglacial marine sedimentation at the core site initiated *ca*. 9.0 cal. ka BP following the retreat of grounded ice. Unstable sea surface conditions subsisted until 7.5 cal. ka BP under the combined influence of warm atmospheric temperatures and proglacial cooling induced by the nearby Innuitian (IIS) and Greenland (GIS) ice sheets. The collapse of the ice saddle in Kennedy Channel at 8.3 cal. ka BP marks the complete opening of Nares Strait and the initial connection between the Lincoln Sea and northernmost Baffin Bay. Delivery of sediment by icebergs was strengthened between 8.3 and 7.5 cal. ka BP following the collapse of the buttress of glacial ice in Kennedy Channel that triggered the acceleration of GIS and IIS fluxes toward Nares Strait. The destabilisation in glacial ice eventually led to the rapid retreat of the GIS in eastern Kane Basin at 8.1 cal. ka BP as evidenced by a noticeable change in sediment source in our core. The gradual decrease of carbonate inputs to Kane Basin between 8.1 and 4.1 cal. ka BP reflects the late deglaciation of Washington Land. The shoaling of Kane Basin can be observed in our record by the increased winnowing of lighter particles as the glacio-isostatic rebound brought the seabed closer to subsurface currents. Our dataset suggests reduced iceberg delivery from 7.5 to 1.9 cal ka BP in relation to the Neoglacial cooling that likely enhanced sea ice occurrence, thus suppressing calving and/or the drifting of icebergs in Nares Strait.

1 Introduction

The Holocene history of Nares Strait, Northwest Greenland, has remained somewhat cryptic despite investigations during the past four decades (e.g. Blake, 1979; Kelly and Bennike, 1992; Mudie et al., 2004; Jennings et al., 2011.). Nares Strait is a key gateway for Arctic sea water and ice toward the Atlantic Ocean, contributing to up to half of the volume of water transported through the Canadian Arctic Archipelago (CAA) which provides fresh water to the Labrador Sea and influences deep water

Clim. Past Discuss., https://doi.org/10.5194/cp-2018-78
Manuscript under review for journal Clim. Past
Discussion started: 11 July 2018

formation (Belkin et al., 1998; Münchow et al., 2006; McGeehan and Maslowski, 2012). Nares Strait supplies one of the most productive regions of the Arctic, the North Water Polynya (NOW), with nutrient-rich Pacific water (Jones et al., 2003; Jones and Eert, 2004) and maintains its very existence by trapping sea and calved glacial ice in ice arches in the north and the south of the strait (Melling et al., 2001; Mundy and Barber, 2001). Despite the importance of Nares Strait, intrinsic investigations into its late Pleistocene history, which is intimately linked with the dynamics of the bordering Innuitian (IIS) and Greenland (GIS) ice sheets, are relatively sparse and much of the knowledge relies on land-based studies. It is now widely admitted that the coalescence of the GIS with the IIS during the Last Glacial Maximum blocked Nares Strait between 19 and *ca*. 8 ^{14}C ka BP (~22-8.5 cal. ka BP). This narrative is supported by the presence of erratic boulders originating from Greenland on Ellesmere Island (England, 1999), by cosmogenic nuclide surface exposure dating (Zreda et al., 1999) and radiocarbon dating on mollusc shells (e.g. Bennike et al., 1987; Blake et al., 1992; Kelly and Bennike, 1992). England (1999) reviewed all land-based evidence available at that time and proposed a complex deglacial history of Nares Strait, featuring the late breakup of glacial ice in central Nares Strait (i.e. Kennedy Channel). These land-based studies have been complemented by Jennings et al. (2011) and Mudie et al. (2004) investigations of marine sediment cores collected in Hall Basin, northernmost Nares Strait. More recently, the geophysical mapping of submarine glacial landforms by Jakobsson et al. (2018) provided additional insight regarding the retreat of Petermann Glacier in Hall Basin. To date, little is known about the downstream consequences of the opening of the Strait, with only two long core records able to provide a marine perspective of the evolution of northernmost Baffin Bay with regards to ice sheet retreat in the area (Blake et al., 1996) and changes in sea ice conditions and marine productivity during deglacial and postglacial times (Levac et al., 2001; Knudsen et al., 2008).

Here we present sedimentological and geochemical data obtained from a 4.25-meter-long marine sediment core retrieved in Kane Basin, central Nares Strait. This core provides a continuous sedimentary record spanning the last 9.0 cal. ka BP, i.e. from the inception of the early Holocene retreat of the GIS and IIS in Nares Strait to modern times. Our set of sedimentological and geochemical records derived from this study offers a unique opportunity to explore the local dynamics of ice-sheet retreat leading to the opening of the Strait and the establishment of the modern oceanographic circulation pattern.

2 Regional settings

Nares Strait is a long (530 km) and narrow channel separating Northwest Greenland from Ellesmere Island, Arctic Canada, connecting the Arctic Ocean to the Atlantic Ocean in Baffin Bay (Fig. 1). Kane Basin is the central, wide (120 km large at its broadest point, totalling an area of approximately 27,000 km²) and shallow (220 m deep) basin within Nares Strait. It separates Smith Sound (600 m deep, 50 km wide) in the south of the Strait from Kennedy Channel (340 m deep, 30 km wide) in the north. A smaller but deeper basin, Hall Basin (800 m deep), where the Petermann Glacier terminates, connects Kennedy Channel to the Robeson Chanel (400 m deep, 21 km wide) in the northernmost sector of the Strait.

The oceanographic circulation in Nares Strait consists of a generally southward flowing current driven by the barotropic gradient between the Lincoln Sea and Baffin Bay (Kliem & Greenberg, 2003; Münchow et al., 2006), while the baroclinic

Clim. Past Discuss., https://doi.org/10.5194/cp-2018-78
Manuscript under review for journal Clim. Past
Discussion started: 11 July 2018

temperature balance generates strong, northerly winds that affect surface layers (Samelson and Barbour., 2006; Münchow et al., 2007; Rabe et al., 2012). The relative influence of the barotropic *vs*. baroclinic factors that control the currents in Nares Strait is highly dependent on the presence of sea ice that inhibits wind stress when landfast (Rabe et al., 2012; Münchow, 2016). Long-term ADCP measurements of flow velocity record average speeds of 20-30 $cm.s^{-1}$ in Kennedy Channel (Rabe et al., 2012; Münchow et al., 2006) and 10-15 $cm.s^{-1}$ in Smith Sound (Melling et al., 2001) with the highest velocities measured in the top 100 m of the water column. Strong currents peaking at 60 $cm.s^{-1}$ have been measured punctually in Robeson Channel (Münchow et al., 2007). The speed of the flow decreases in the wider sections of Nares Strait, and a northward current has been shown to enter Kane Basin from northern Baffin Bay (Bailey, 1957; Muench, 1971; Melling et al., 2001; Münchow et al., 2007). Temperature and salinity isolines imply that an anti-clockwise circulation takes place in the surface layers of Kane Basin, while the deeper southward flow of Arctic water is channelled by bottom topography and concentrated in the basin's western trough (Muench, 1971; Moynihan, 1972; Münchow et al., 2007).

Sea ice concentration in Nares Strait is usually over 80% from September to June (Barber *et al*., 2001). The state of the ice varies between mobile (July to November) and fast-ice (November to June). The unique morphology of the Strait leads to the formation of ice arches in Nares Strait when sea ice becomes landfast in the winter. The ice arches are a salient feature in the local and regional oceanography of Nares Strait: they control the export of low salinity Arctic water into Baffin Bay (Münchow, 2016) and sustain the existence of the NOW Polynya (Barber et al., 2001). The main iceberg sources for the strait are Petermann Glacier in Hall Basin, and Humboldt Glacier in Kane Basin, both associated to the GIS.

The Greenland coast bordering Kane Basin is relatively flat. In Inglefield Land the Precambrian basement is exposed, displaying supracrustal crystalline rocks and metamorphic rocks, essentially reported as aluminous metasediments and gneisses or granitoid gneisses, with some references to quartizite (Koch, 1933, Dawes, 1976, 2004; Harrison and Oakley, 2006 and references therein). Dawes (2004) postulated that this Precambrian basement also underlies the 100 km wide Humboldt Glacier. To the north, the Precambrian basement in Washington Land is overlaid by Cambrian, Ordovician and Silurian dolomites, limestones and evaporites (Koch, 1929a, b; Harrison et al., 2006 and references therein). The Ellesmere shore of Kane Basin rises abruptly from sea level and is punctured by narrow fjords, penetrating inland for nearly 100 km (Kravitz 1982). In southern Kane Basin, the same Precambrian crystalline rocks outcrop to form the Ellesmere-Inglefield Precambrian Belt. The central and northern sectors of Ellesmere Island's coast mainly comprise Cambrian to Devonian carbonates and evaporates. Fluviodeltaic quartz sandstone, volcanistic sandstone, minor arkose and sometimes coal are found in the Paleogene Eureka Sound sequence that occurs along the western coast of Kane Basin, on the Ellesmere Island flank of Kennedy Channel and on Judge Daly Promontory (Christie, 1964, 1973; Kerr, 1967, 1968; Miall, 1982; Oakey and Damaske, 2004). Coal bearing Paleogene clastics also occur along the coast of Bache Peninsula and in morainic deposits on Johan Peninsula in south-western Kane Basin (Kalkreuth et al., 1993).

Kravitz (1976) described modern sedimentation in Kane Basin according to three main provinces defined on the basis of mineralogical and grain size characteristics. The first province covers the eastern, central and southern part of the basin in which the predominant crystalline clay and silt sediments are water-transported off Humboldt Glacier and Inglefield Land.

The second province, in the west of the basin, includes a higher fraction of ice-transported materials, mostly carbonates with clastic debris occurring in the deeper trough. Northern Kane Basin makes up the third province in which water-transported, mostly carbonate sediments from Washington Land, are deposited in its northernmost part, while ice-transported crystalline particles are more common in the southern part of this province.

2 Material and methods

Sediment core AMD14-Kane2b was retrieved at 217 m water depth in Kane Basin, Nares Strait (79°31.140'N; 70°53.287'W) during the 2014 ArcticNet expedition of the CCGS *Amundsen*. This core was collected with a wide-square section (25 cm x 25 cm) gravity corer (Calypso Square CASQ) and immediately sub-sampled on-board using large U-channels.

3.2 Sedimentological analyses

The description of the various lithofacies was based on the visual description of the core and high-resolution images using a computed tomography (CT) scanner (Siemens SOMATOM Definition AS+ 128 at INRS, Quebec, Canada). Changes in sediment density were estimated from variations in the CT-numbers which were processed according to Fortin et al. (2013). To complement CT analyses, a series of thin sections covering two intervals were sampled across major lithological changes toward the base of the core (425-405 cm and 373.5-323.5 cm) in order to visualise the internal structure and examine the nature of these facies. The thin sections were prepared according to Zaragosi et al. (2006). Grain size analyses were performed at intervals of 2 to 4 cm throughout the archive. A Malvern 2000 laser sizer was used to determine the relative contribution (expressed as % of particles) of clay and colloids (0.04-4 µm), silt (4-63 µm) and sand (63-2000 µm) within the < 2 mm fraction. The same samples were also subjected to wet sieving through 63, 125 and 800 µm meshes in order to determine the weight fraction of sands and identifiable ice-rafted debris (IRD), expressed as % weight of the bulk dry sediment.

3.3 XRF core-scanning

High-resolution (0.5 cm) X-Ray Fluorescence (XRF) scanning was conducted along the archive using an AVAATECH XRF core-scanner. The semi-quantitative elemental composition of the sediment was measured throughout the whole archive with the exception of two units which contain large clasts. Measurements were acquired with generator settings of 10, 30 and 50 kV in order to detect elements in the range of Al to Ba. Raw XRF data for each element were normalized to the sum of XRF counts of all elements except Rh and Ag whose counts are biased during data acquisition (Bahr et al., 2014) in order to correct for changes induced by down-core variations in grain size and/or water content (Tjallingii et al.., 2007).

In this study, we use the elemental signature as an indication of the sediment sources for detrital material. The sedimentary rocks from northern Kane Basin and Nares Strait are typically rich in Ca, whereas higher concentrations of Si and K characterize the crystalline rocks of the Ellesmere-Inglefield Precambrian Belt. Additionally, heavy elements Ti and Zr reflect

Clim. Past Discuss., https://doi.org/10.5194/cp-2018-78
Manuscript under review for journal Clim. Past
Discussion started: 11 July 2018

the grain size variation in the core as they are commonly enriched in coarser particles (Correns, 1954 ; Pedersen et al., 1992 ; Ganeshram et al., 1999 ; Bahr et al., 2014).

3.3 Chonology and age model

The chronology is based on a set of twenty radiocarbon ages obtained from mixed benthic foraminifera samples and unidentified mollusc shells. Only one mollusc fragment was dated (at 301.5 cm) and yielded an age of >43 ka and is thus clearly remobilised (Table 1). The core top is dated at -5 years BP (1955 AD) based on ^{210}Pb measurements and a comparison with the ^{210}Pb profile (Supplementary Figure S.1) obtained from a box core collected at the same coring site.

Reservoir ages in Nares Strait are difficult to assess owing to the scarcity of pre-bomb specimens in collections of marine shells from the area. Only three molluscs were dated in Nares Strait with ΔR ranging between 180 and 320 years, comparing relatively well with molluscs from the western sector of northernmost Baffin Bay (ΔR of 140 and 270), while molluscs collected near Thule, North-western Greenland, yielded negative ΔR (McNeely et al., 2006). Coulthard et al. (2010) proposed a regional ΔR for the CAA of 335 years based on the McNeely et al. (2006) dataset of pre-bomb radiocarbon dated molluscs and taking into account the general oceanographic circulation in the CAA. However, unlike in other passages of the CAA which present shallow sills at their southern extremities, younger Atlantic water from Baffin Bay enters Nares Strait – or at least Kane Basin – from the south (Bailey, 1957; Muench, 1971; Münchow et al., 2007). We thus choose to correct ^{14}C ages in this study with the average ΔR of the three pre-bomb collected mollusc shells in Nares Strait, i.e. 240 years, bearing in mind that reservoir ages are likely comprise between 0 and 335 years and may have changed through time as a consequence of the major oceanic reorganisation undergone in Nares Strait. Radiocarbon dating in Nares Strait is further complicated by the proximity of old carbonate rocks that are prone to introducing additional uncertainties in the ^{14}C ages yielded by deposit-feeding molluscs (England et al., 2013). The non-systematic discrepancies between ages yielded from deposit-feeders and those from suspension-feeding molluscs – the so-called *Portlandia* effect (England et al., 2013) – cannot be corrected. However, this represents a greater challenge for landbound studies that pinpoint the timing of the deglaciation of a given location based on the oldest mollusc found in that location. *A contrario*, when establishing the age model of sediment cores, the age *vs*. depth relationship reveals any outliers that can be identified as being either (1) remobilised by ice-rafting, slumping or bioturbation, or (2) potentially affected by the *Portlandia* effect. Hence, we deem the *Portlandia* effect to be of minor concern in the establishment of the age model in this study despite the possible inclusion of deposit-feeders in our radiocarbon dataset. The ^{14}C ages were calibrated with the Marine13 curve (Reimer et al., 2013) using Calib7.1 (Stuiver et al., 2018) with a marine reservoir age correction of 640 years (ΔR=240). We computed an age/depth model for core AMD14-Kane2b based on radiocarbon-dated material using CLAM 2.2 (Blaauw, 2010), and assuming that a 20 cm long clast-rich deposit (300-320 cm) was deposited near instantaneously at the scale of our chronology.

According to our chronology, core AMD14-Kane2b covers the last 9.0 cal. ka BP (Fig. 3). Drastic changes in depositional environments, most particularly during the time interval corresponding to the lower half of our sediment core, explain the wide

Clim. Past Discuss., https://doi.org/10.5194/cp-2018-78
Manuscript under review for journal Clim. Past
Discussion started: 11 July 2018

range of sedimentation rates. High sedimentation rates are observed between the base and ~250 cm where they decrease from ~220 cm.ka^{-1} to 30 cm.ka^{-1}, and after which sedimentation rates increase to reach 50 cm.ka^{-1} at 120 cm before decreasing again to ~20 cm.ka^{-1} at the top of the core.

4 Results and interpretations

The comparison of the ^{210}Pb profiles of core AMD14-Kane2b and the box core collected at the same location reveals the relatively good preservation of the topmost sediments in the CASQ core permitted by the large diameter of this corer (sediment loss of ~5 cm, Supplementary Figure S.1). We therefore place the top of core AMD14-Kane2b at the interface in the seismic profile (Fig. 4). Assuming an acoustic velocity of 1500 m.s^{-1}, the base of the core reached a coarse unit (unit 0) shown to continue below the retrieved sediment for several meters (Fig. 4), which is likely to have stopped the penetration of the CASQ corer. The high level of backscatter, discontinuous reflectors and lack of internal coherence in unit 0 are all discriminant acoustic characteristics of diamicton which contains high amounts of unsorted clasts in a clay to silt matrix (Davies et al., 1984). Given the thickness of unit 0, we interpret this diamicton as being either subglacial till or the first glacimarine sediments deposited during the retreat of the marine-based ice sheet margin.

Based on CT-scans and grain size records, five lithological units were defined for core AMD14-Kane2b, each corresponding to specific depositional environments (Fig. 5, Table 2). The sedimentological processes at play will be examined here, while their environmental significance will be considered in the discussion section of this paper. The elemental composition of the sediments is largely dominated by Ca throughout the core. Although contributing to a minor extent to the elemental XRF record, temporal variations in K abundances reflect changes in sediment sources.

Unit 1 (425-394 cm, ca. 9.0 cal. ka BP) encompasses three subunits of distinct lithological nature.

Subunit 1A (425-416 cm) consists of high density, occasionally sorted coarse sediment in a clayey matrix, interbedded with thinner layers of lower density silty clay (Table 2). The base of the coarser laminations show erosional contact with the underlying finer beds (thin sections in Table 2). Grain size analysis reveal large amounts of sand (26-39%) and silt (24-32%) in the <2 mm fraction in this interval. The relative weight of the 125-800 µm and >800 µm fractions also contribute considerably to the overall weight of the sediment (18% and 11%, respectively).

These laminated deposits display all the characteristic of alternating meltwater pulses and/or ice-proximal turbidity current deposits (coarser bands) with plume deposits (finer bands) (List, 1982; Ó Cofaigh and Dowdeswell, 2001). Unit 1A was most likely deposited at the ice sheet margin some ~9.0 cal. ka ago, according to a dated mollusc shell at the base of unit 1C and given the very high sedimentation rates in ice-proximal environments.

Subunit 1B (416-410 cm) displays a sharp decrease in sediment density with the replacement of sand by finer material (60% clay in the <2 mm fraction, Fig. 5, Table 2). XRF data for subunit 1B show low counts of Ca and K whereas Ti counts are high.

Clim. Past Discuss., https://doi.org/10.5194/cp-2018-78
Manuscript under review for journal Clim. Past
Discussion started: 11 July 2018

The finer grain size in this subunit is indicative of a change from an ice margin to an ice-proximal glacimarine environment where suspended matter settling from turbid meltwater plumes is likely the main depositional process (Elverhøi et al., 1980; Syvitstki, 1991, Dowdeswell et al., 1998; Hogan et al., 2016), although the limited thickness (4 cm) of subunit 1B is rather unusual for this process. High Ti counts suggest a high energy environment, supporting the previous hypothesis of an ice marginal environment where meltwater pulses can transport relatively large particles. The intermediate abundance of Ca and K do not point to any specific source of materiel, but rather a mixture of sediments of eastern (gneiss) and north-western (carbonate) origin (Fig. 2).

Subunit 1C (410-394 cm) interrupts the fine grained sedimentation with a sharp increase in the occurrence of outsized clasts. The coarser fractions account for a significant part of the sediment (up to 18% for both the >800 and 800-125 µm fractions) within a dominantly clayey matrix. Sediment density in subunit 1C increases to reach values similar to those observed in subunit 1A. However, unlike subunit 1A, subunit 1C is not laminated and clasts are larger (frequent gravel) and ungraded.

Given the high gravel content in subunit 1C, we consider that the clasts were predominantly iceberg-rafted to the core location rather than sea-ice rafted (Pfirman et al., 1989; Nürnberg et al; 1994). These large amounts of IRD among very poorly sorted material can be interpreted as (1) increased iceberg calving rates, (2) changes in the delivery of sediment by icebergs (increased melting of or dumping from icebergs) or (3) a severe decrease in the delivery of finer particles that increases the apparent contribution of clasts to the sediment (Hogan et al., 2016 and references therein).

Unit 2 (394-320 cm, 9.0-8.3 cal. ka BP) can be divided into two subunits based on grain size and density. The relative weight of the coarse fraction oscillates throughout unit 2 with a generally decreasing trend.

Subunit 2A (394-370 cm, 9.1-8.8 cal. ka BP) is composed of poorly sorted, bioturbated sediment (~55% clay and ~38% silt in the <2 mm fraction) with varying contributions of coarser material (between ~0 and 5%) and occasional lonestones (Fig. 5, Table 2). Sediment density is fairly high, but gradually decreases toward the top of subunit 2A. Ti counts decrease gradually in this subunit, mirroring the decrease in density. The base of subunit 2A is rich in Ca and relatively poor in K. The abundances of these elements evolves gradually with opposing trends as K increases and Ca decreases upward in this subunit.

The dominance of fine particles in subunit 2A points to a delivery by meltwater plumes that includes occasional iceberg-rafted debris. The decreasing Ti counts and silt content along with increasing clay suggests a growing distance of the ice margin from the core site since coarser silt and Ti-bearing minerals settle closer to the ice margin, while clay particles tend to sink in more ice-distal locations (Dowdeswell et al., 1998; Ó Cofaigh and Dowdeswell, 2001). The high Ca content at the base of subunit 2A indicates that the origin of this meltwater-transported material is the Paleozoic carbonates on Ellesmere Island in western Kane Basin and/or Washington Land in northern Kane Basin (Fig. 2). An upward increase in the contribution of gneissic K from eastern Kane Basin probably reflects a gradual change in the sedimentary source.

The sediments of subunit 2B (370-320 cm, 8.9-8.3 cal. ka BP) have a lower density and a lower sand and silt content than those of subunit 2A, while clay content reaches maximum values to an average 63%. Scarce lonestones occur in this subunit and the sediment appears to be faintly laminated. Four biogenic carbonate samples, both mollusc and mixed benthic foraminifera samples, were dated in subunit 2B and high sedimentation rates of ~130 $cm.ka^{-1}$ decreasing upward to 90 cm.ka-

[1] were calculated from the age model (Table 1, Fig. 3). The elemental signature of subunit 2B is rather stable with low Ti, relatively low Ca and high K counts.

These high sedimentation rates, substantial concentrations of clay and the slightly laminated aspect of subunit 2B indicate that these sediments were mainly delivered by meltwater plumes in a more distal glacial setting (Ó Cofaigh and Dowdeswell, 2001). A significant portion of these sediments derived from eastern Kane Basin gneisses.

Unit 3 (320-300 cm, 8.3 cal. ka BP) stands out as clast-rich interval. The high density of this unit is comparable to that of subunits 1A and 1C. CT-scans and thin sections reveal the presence of a finer grained horizon enclosed between coarser material, dividing this interval into three subunits (Table 2).

Subunit 3A (320-313 cm) corresponds to the lower clast-rich subunit. A significant portion of the bulk sediment is attributed to 800-125 µm sand (17% wt) and >800 µm sand (up to 7% wt), while the clay matrix contributes to ~53% of the <2 mm fraction. Ti and Ca counts are relatively high whereas K counts have significantly decreased compared to the underlying subunit 2B (Fig. 5).

The high clast content and absence of grading suggest that the sediments forming subunit 2B were ice-rafted and deposited at the core location (Ó Cofaigh and Dowdeswell, 2001). The predominant carbonate (Ca) material in this subunit likely originates from northern and/or western Kane Basin.

Faint laminations are visible on the CT-scan images of subunit 3B (313-305 cm). The sediment of this subunit is composed essentially of clay and silt (47 and 43% respectively) with a relatively low sand content (<10 % in the <2 mm fraction and each of the coarser fraction represents less than 3% of the sediment weight). Ca counts are high in subunit 3B and Ti and K counts are relatively low in comparison to the rest of the core. Analysis of the sieved residues revealed the presence of benthic foraminifera in this subunit which were picked and dated at ~9.4 ^{14}C BP (9.9 cal. ka BP with ΔR=240, Table 1).

The poor sorting of subunit 3B could possibly indicate that they were ice-transported, but the near absence of clasts (e.g. in contrast to the overlaying and underlying subunits of interval 3) contradicts this hypothesis. The modest contribution of clay along with the relatively high silt content rather points to the transport and deposition of these sediments by a high velocity current. The elemental signature of this subunit (predominantly carbonate) denotes a northern and/or western Kane Basin origin. Concerning the old age yielded from the mixed benthic foraminifera picked in this subunit, the age model shows that these foraminifera were remobilised. It is possible that a small quantity of pre-Holocene foraminifera was mixed in with living fauna. This would imply that sediments pre-dating the last glaciation (>22 cal. ka BP) were preserved under the extended GIS and IIS in Nares Strait, and were eroded and transported to the core site during the deposition of subunit 3B. An alternative explanation is that the sample is composed of postglacial specimens of a similar age which were eroded from the seabed and transported to the site.

Subunit 3C (305-300 cm) contains large amounts of coarse material with an average of 44 % sand and only 32 % clay in the <2 mm fraction. The sand in this subunit is coarser than in 3A with the 800-125 µm fraction contributing to ~34% of the total sediment while up to a further 10% of the sediment weight is accounted for by the >800 µm fraction. Ti counts are high in subunit 3C while Ca and K counts are relatively low (Fig.5).

Clim. Past Discuss., https://doi.org/10.5194/cp-2018-78
Manuscript under review for journal Clim. Past
Discussion started: 11 July 2018

The very high clast content of subunit 3C along high Ti counts and the absence of grading are indicative of iceberg-rafting and deposition. The shell fragment that was dated in the topmost horizon of this subunit (>42 ^{14}C BP) was clearly remobilised, likely by ice-rafting. The sediment forming subunit 3C appear to originate from both carbonates in northern and/or western Kane Basin and from gneisses in eastern Kane Basin (Fig. 2). The age model points to rapid sedimentation of unit 3 with an age of 8.22 cal. ka BP on mixed benthic foraminifera picked from the horizon directly above unit 3, and an age of 8.38 cal. ka BP in a sample 7 cm below the base of unit 3 that extrapolates to ~8.29 cal. ka BP at 320 cm in the age model (Table 1, Fig. 3).

Unit 4 (300-280 cm, 8.3-8.1 cal. ka BP) has a similar density and clay content (~58 %) to subunit 2B. The contribution of sand in these sediments are however higher than in subunit 2B with ~6.5 % weight accounted for by >125 µm sand and ~14 % sand in the <2 mm fraction. The elemental composition of unit 4 is also fairly similar to that of subunit 2B. Although slightly higher than in subunit 2B, Ca counts are relatively low and increase discreetly toward the top of this unit. K counts are high and Ti counts are low (Fig. 5).

The high clay content of unit 4 suggests that delivery from meltwater plumes was the dominant sedimentary process at play during this time interval. The substantial amount of sand in this unit indicates that a significant proportion of the sediment was also ice-rafted to the location. As previously mentioned, the increase in ice-rafted debris can indicate (1) increased calving rates when originating from iceberg-rafting, (2) changes in iceberg delivery of sediment (increased melting or dumping of icebergs) or (3) a decrease in the delivery of finer particles that increases the apparent contribution of clasts to the sediment (Hogan et al., 2016 and references therein). The high sedimentation rates (~90 cm.ka^{-1} from the age model and ~190 cm.ka^{-1} from the linear interpolation between the dates at 297.5 cm (8.22 cal. ka BP) and 273.5 cm (8.09 cal. ka BP), Table 1, Fig. 3) support this narrative of delivery by meltwater and ice-rafting that are typically responsible for the transport and deposition of large quantities of sediment (Svenden et al., 1992, Dowdeswell et al., 1998), while seemingly excluding the possibility of a significant decrease in the delivery of finer particles. A notable portion of the sediments originates from the Precambrian gneisses of eastern Kane Basin while the contribution of northern and/or eastern carbonates increases slightly throughout this interval.

Sediments in the <2 mm fraction forming unit 5 (280-0 cm, 8.1-0 cal. ka BP) differ significantly from those of previous units (Fig. 5). The clay content drops to steady, lower values (49% on average) and the CT-scans show a generally homogenous sediment with frequent traces of bioturbation. Changes in grain size divide unit E into two subunits.

The sediments in subunit 5A (280-250 cm, 8.1-7.5 cal. ka BP) contain a relatively high proportion of sand peaking at 12 % in the <2 mm fraction, while the combined contribution of the coarser fractions averages at ~5.5 % weight. Lonestones occur frequently and are visible in the CT-scan images.

K counts drop sharply at the base of subunit 5A and are mirrored by an equally sudden increase in Ca counts. Ti counts are low, but increase very discreetly toward the top of this subunit.

The significant decrease in clay particles in subunit 5A compared to units 4 and 2B suggests that delivery from meltwater plumes was reduced in this interval, either in relation to a decrease in glacial melting rates or to a more ice-distal setting. The

Clim. Past Discuss., https://doi.org/10.5194/cp-2018-78
Manuscript under review for journal Clim. Past
Discussion started: 11 July 2018

scarcity of clasts in this subunit can be explained by a change in the sea-ice regime and/or the counterparts of the aforementioned hypothesis presented in Hogan et al., 2016, i.e. (1) decreased iceberg calving rates or (2) decrease iceberg melting. It is not unreasonable to rule out hypothesis 3 (i.e. increased contribution of finer particles) given the reduced contribution of the finer particles in the <2 mm fraction and the decrease in sedimentation rates from 60 to 40 cm.ka^{-1} in this subunit. There is a marked change of sediment source at the base of subunit 5A as the delivery of gneiss material to the core location drops abruptly and is replaced by strengthened contributions of northern and/or western carbonates (Fig. 5).

Subunit 5B (250-0 cm, 7.5-0 cal. ka BP) is generally homogenous with lonestones occurring sporadically throughout. The silt content increases gradually from ~40 to ~47 % toward the top of the core. The contribution of the coarser fractions to the total sediment weight is fairly stable from the base to ~40 cm (1.9 cal. ka BP), where the 63-125 µm and >125 µm fractions account for ~2% and <1% of the total sediment weight, respectively. The relative weight of the 63-125 µm sand fraction doubles to ~4% in the top 40 cm of the core (Fig.5). K counts are low and stable throughout subunit 5B. Ca counts, previously high in subunit 5A, decrease gradually until ~120 cm (~4.1 cal. ka BP) after which they remain relatively low until the core top. Ti counts increase progressively until ~80 cm (3.2 cal. ka BP) where they then plateau to higher values.

Most of the age reversals in our age model occur in this subunit (Table 1, Fig.3). Two whole mollusc shells yielded a younger age than expected for their respective core depths and were likely remobilised by bioturbation. A sample of mixed benthic foraminifera yielded a radiocarbon age some 2 ka older than expected. This sample probably contains a mixture of coeval and remobilised foraminifera (either by bioturbation or by water/ice transport from another location).

The overall limited contribution of the coarser fractions to the sediment of subunit 5B in comparison to the underlying lithologic units indicates that ice-delivery of sediment was reduced during this interval. Furthermore, the relatively low amounts of clay imply that meltwater delivery was also weakened. The sediments of subunit 5B were likely primarily water-transported to the core site (Hein and Syvitski, 1992; Gilbert, 1983). The increase in silt and Ti toward the top of the core suggest winnowing by an increase in bottom current (Correns, 1954 ; Pedersen et al., 1992 ; Ganeshram et al., 1999 ; Mulder et al., 2013, Bahr et al., 2014). Relatively low sedimentation rates (20-50 cm.ka^{-1}) corroborate the narrative that delivery from meltwater plumes was limited in favour of a more hemipelagic sedimentation regime, also supported by the visible bioturbation in this subunit. The increase in fine sand in the most recent sediment may be due to a resumption of ice-rafting over the last 1.9 cal. ka BP. The contribution of carbonates from northern and/or western Kane Basin as a primary sediment source diminishes gradually between ~270 cm (~7.9 cal. ka BP) in subunit 5A and ~120 cm (~4.1 cal. ka BP) in subunit 5B after which it remains stable until the top of the core.

5 Discussion

Our study of core AMD14-Kane2b has enabled us to reconstruct a succession of depositional environments in Kane Basin following the retreat of the formerly coalescent GIS and IIS in Nares Strait (Fig. 6). Here we discuss our reconstructions in the

light of other paleoceanographic and paleoclimatic studies to provide a broader view of the Holocene history of Nares Strait (Fig. 6 and Table 2).

The presence of erratic Greenland boulders on Ellesmere Island from Kennedy Channel to the northern entrance of Nares Strait attest to the coalescence of the IIS and GIS along the western side of northern Nares Strait during the Last Glacial Maximum (LGM) (England, 1999). The absence of such erratics along the western and southern coasts of Kane Basin implies that the confluence of the two ice sheets laid further at sea in the southern half of the strait, at least until Smith Sound where asymmetric bathymetric features suggest that southward flowing Greenland ice may have reached Ellesmere Island (Blake et al., 1996). Radiocarbon dating on samples from raised beaches provides minimum ages for marine ingress in Nares Strait. These ages are older in the northern and southern extremities of the Strait, while only younger ages are yielded by samples in northern Kane Basin and Kennedy Channel implying that a central (grounded) ice saddle persevered longer in the shallower sector of the Strait (England, 1999 and references therein; Bennike, 2002). In addition to providing minimum ages for ice sheet retreat, ^{14}C dating on marine derived material in raised beaches enables one to identify the former shoreline and assess the glacio-isostatic readjustment of the continental crust. However, this approach can only provide minimum ages for (glacial ice-free) aquatic environments at a given place and time and does not necessarily correspond to the position of the ice margin which can be several kilometres inland. Cosmogenic nuclide surface exposure dating is an efficient method to temporally constrain inland ice sheet retreat. However, such investigations are scarce in Nares Strait: only one study documents the glacial retreat on Hans Island, off Greenland in Kennedy Channel (Zreda et al., 1999). England's (1999) paleogeographical maps of ice sheet retreat in Nares Strait based on radiocarbon dated molluscs were revised in Fig. 6 where the offshore limits for the GIS and IIS are proposed based on our sedimentological and geochemical data from core AMD14-Kane2b. The continuous nature of our record also allows us to propose a more precise chronology of the deglaciation of central Nares Strait.

5.1 *Ca*. 9.0 cal ka BP: ice sheet retreat in Kane Basin

Our archive demonstrates that marine sedimentation took place in Kane Basin as early as ~9.0 cal. ka BP. Grain size characteristics and sedimentary structures suggest that the laminated basal unit (1A) represents the topmost deposits in the ice marginal environment shortly after ice sheet retreat at the core site (Fig. 6, Table 2). The settling of meltwater plume sediments in the proximal glacial marine environment that followed (1B) is devoid of IRD and seems to have been interrupted by an iceberg-rafted interval (1C). The absence of molluscs pre-dating 8.8 cal. ka BP in Kane Basin (England, 1999) likely indicates that following the deglaciation of Smith Sound *ca*. 9.9 cal. ka BP (Fig.6, England, 1999), ice sheet retreat in Kane Basin occurred off the current coast where melting was potentially enhanced by the increasing influence of warmer Atlantic water from the West Greenland Current after 10.9 cal. ka BP, $\Delta R = 0$ (Funder 1990; Kelly et al., 1999; Knudsen et al., 2008). Based on the sedimentary properties of subunit 1A, we propose that *ca*. 9.0 cal ka BP, the GIS/IIS ice margin was located at the core site, completing the offshore area of England's (1999) paleogeographical map for this period (Fig. 6). Calving and delivery of IRD from icebergs would be expected in ice-proximal location (e.g. Ó Cofaigh et al., 2001), however the fine laminated structure and absence of IRD in subunit 1B suggest that calving was temporarily suppressed by the presence of sea ice fastened

to the ice GIS/IIS margins. Such interpretations have been made in a number of studies where clasts are absent from ice-proximal glacimarine sediments (e.g. Osterman and Andrews, 1983; Dowdeswell 1994, 2000). Following sea ice breakup, calving activity has been documented to be intensified by the release of accumulated glacial ice flux (Reeh et al., 2001) hence explaining the large amount of iceberg-rafted debris in subunit 3C. Laurentide Ice Sheet readvances have been documented through the dating of end and lateral moraines on Baffin Island aged between 9 and 8 cal. ka BP (Andrews and Ives, 1978) and have been linked to colder periods. A particularly cold event *ca*. 9.2-9.3 cal. ka BP, which is reported in the regional literature from ice core (Vinther et al., 2006, Fisher et al., 2011) and lacustrine records (Axford et al., 2009), may have enhanced sea ice occurrence during the deposition of subunit 1B. Reservoir ages in Kane Basin are likely to have been reduced prior to the collapse of the IIS/GIS ice saddle in Kennedy Channel and the arrival of poorly ventilated Arctic water. The age of unit 1 with ΔR=0 is 9.3 cal. ka BP which suggests to us that subunit 1B could well have been deposited during the 9.2-9.3 cal. ka BP cold event, followed by sea ice break up and the release of icebergs (1C).

5.2 9.0-8.3 cal. ka BP: ice proximal to ice distal environment in Kane Basin

The increasingly finer particles that compose unit 2 suggest a growing distance between the core site and the ice margin. The dominant sedimentary process at play is settling from meltwater plumes which is typically responsible for high sedimentation rates, along with frequent delivery of IRD (Table 2). The Early Holocene was characterised by high atmospheric temperatures during the Holocene Thermal Maximum (HTM) occasioned by greater solar insolation (Bradley, 1990). The HTM has been defined for the eastern sector of the CAA as the period between 10.7 and 7.8 cal. ka BP based on the Agassiz ice core record (Lacavalier et al., 2017). The high melting rates of the ice sheets during the HTM (Fisher et al., 2011) likely enhanced the delivery of particles by meltwater and contributed to the high sedimentation rates observed in our core. More distant glacial ice from the site is also in good agreement with the occurrence of molluscs dated between 8.8 and 8.3 cal. ka BP on Ellesmere Island and northwest Greenland (Fig. 6, England et al., 1999). The elemental signature of subunit 2B suggests however that the GIS was still present in eastern Kane Basin and delivered material derived from the gneiss basement to the core site. The volcanic clastics on Ellesmere Island may also have contributed to K counts in our geochemical record, but we consider their input marginal given the limited surface of this geological unit compared to the gneiss and crystalline basement which outcrops in much of Inglefield Land and underlays Humboldt Glacier. Furthermore, the IIS was a cold base ice sheet (e.g. Tushingham, 1990, Dyke, 2002) and as such likely delivered overall less sediment from meltwater than the warm-based GIS. The occurrence of IRD in unit 2 implies that relatively open water conditions occurred during this interval, enabling icebergs to drift in Kane Basin. This is in good agreement with low sea ice concentrations reported nearby in Lancaster Sound (from 10 to 6 cal. ka BP, ΔR=290 Vare et al., 2009; from ~10-7.8 cal. ka BP, R=335 Pienkowski et al., 2012). However, while the decreasing trend of the coarse fraction in unit 2 may indicate more stable sea ice conditions toward the end of the interval, fluctuations in the coarse fractions in our record suggest that sea ice conditions were variable. This is in line with both decreasing atmospheric temperatures towards the end of the HTM (Lecavalier et al., 2017) and Knudsen's et al. (2008) observations of unstable conditions between 9.5 and 8.2 cal. ka BP in northernmost Baffin Bay.

Clim. Past Discuss., https://doi.org/10.5194/cp-2018-78
Manuscript under review for journal Clim. Past
Discussion started: 11 July 2018

5.3 8.3 cal. ka BP: the opening of Kennedy Channel

Unit 3 appears to be primarily iceberg-rafted, with an inclusion of a finer, water-transported silty subunit (3B). A foraminifera-derived radiocarbon age obtained from subunit 3B (Table 1) suggests sediment remobilisation within this time interval. Microscopic observations revealed that these foraminifera were well preserved, indicating that the sample is unlikely to include pre-glacial specimens. Since these foraminifera are predominantly postglacial and considering that most of Kane Basin was under grounded ice until ~9.0 cal. ka BP, it is highly unlikely that these foraminifera dated at 9.9 cal. ka BP (ΔR=240, ~9.4 ^{14}C BP) originated from northern Kane Basin. Given the relatively low bottom current velocities in Smith Sound (currently <10 cm.s^{-1}, Münchow et al., 2007) it is also unlikely that they were transported from southern Nares Strait. Jennings et al. (2011) observed foraminifera dated at 9.8 cal. ka BP (ΔR=240, 9.3 ^{14}C BP) in a sediment core from Hall Basin. These glacimarine sediments and fauna imply that northern Nares Strait was ice-free at that time. If we consider that unit 3A was deposited by the passing over Kane Basin of glacial ice having broken-up in Kennedy Channel, then a plausible origin for unit 3B could be the entrainment of sediment from northern Nares Strait associated with the discharge of large amounts of water as the connection was established. The absence of any molluscs in Kennedy Channel pre-dating 8.1 cal. ka BP further suggests that Kennedy Channel was still blocked until then, although this method can only provide minimum ages for ice sheet retreat. The onset of decreasing landfast sea ice on the northern coast of Ellesmere Island and northern Greenland after 8.2 cal. ka BP (England et al., 2008; Funder et al., 2011) may have been associated with the flushing of ice through Nares Strait after the opening of Kennedy Channel. Given the excellent correspondence between the aforementioned evidence, we consider that subunits 3A and 3B were deposited as the ice saddle in Kennedy Channel broke-up. The high carbonate signal in the elemental data (Fig. 5) also suggests that the sediments from subunits 3A and 3B originated from northern Nares Strait (Fig. 2).

The sediment source of subunit 3C appears less evident with a lower Ca and a higher K (gneiss) content, although the dominant depositional process is clearly iceberg-rafting based on the abundance of clasts in this interval. The elemental composition of subunit 3C suggests that the sedimentary material is not exclusively of northern Nares Strait origin, but also originates from the GIS in eastern Kane Basin (Fig. 2). Investigations into the internal stratigraphy of the GIS and their comparison to north Greenland ice cores have demonstrated that the collapse of the ice saddle in Kennedy Channel triggered the acceleration of glacial fluxes along Nares Strait (MacGregor et al., 2016). The destabilisation of the GIS following the collapse of the ice saddle may have provoked intense calving that led to the deposition of subunit 3C.

5.4 8.3 - 8.1 cal. ka BP: Increase iceberg delivery to Kane Basin

The abundance of iceberg-rafted debris has increased considerably in unit 4 compared to unit 2. This is likely the result of the aforementioned acceleration of the GIS and IIS along Nares Strait following the collapse of the ice saddle in Kennedy Channel (MacGregor et al., 2016), as well as the arrival of icebergs from new sources to Kane Basin situated in northern Nares Strait. The presence of IRD during this interval suggests that sea ice occurred infrequently in Kane Basin, in agreement with more open surface conditions as evidenced in the nearby Barrow Strait (Vare et al., 2009; Pienkowski et al., 2012). The high gneiss

signal in the elemental composition implies that the GIS was still relatively close to our core site and had not yet retreated in eastern Kane Basin, contributing to the high sedimentation rates recorded in this unit.

5.5 8.1-7.5 cal. ka BP: Rapid retreat of the GIS in Kane Basin

The abrupt decrease in the gneiss signal of the elemental composition implies that the GIS retreated rapidly in eastern Kane Basin at *ca*. 8.1 cal. ka BP (Fig.6), likely in relation to the removal of the glacial buttress in Kennedy Channel (unit 3). The subsequent decrease in the >125 µm fraction may be associated with the outset of the deceleration of glacial fluxes along Nares Strait, as well as more distant glacial ice in eastern Kane Basin resulting from the retreat of the GIS. Reduced calving may also have been promoted by increased sea ice occurrence following the termination of the HTM. Heavier sea-ice conditions after 7.8 cal. ka BP (ΔR=335) has indeed been reported in nearby Lancaster Sound (Pienkowski et al., 2012).

5.6 7.5-0 cal. ka BP: deglaciation of Washington Land, suppressed iceberg-rafting and implications on the development of the NOW Polynya

The high Ca counts at the beginning of this interval are likely related to the erosion and delivery of material from Washington Land and a decrease in the delivery of crystalline material by the GIS (Fig. 5). The progressive decrease in Ca counts between 7.5 and 4.1 cal. ka BP can be linked to the deglaciation of Washington Land. The oldest molluscs found on the southern coast of Washington Land are dated between 7.8 and 7.4 cal. ka BP, while specimens found in morainic deposits imply that the extent of the GIS reached a minimum between 4 and 0.7 cal. ka BP (Fig. 6, Bennike, 2002). Increasing silt and Ti counts in our core suggest winnowing by stronger bottom water currents. We propose that as the glacio-isostatic rebound lifted the continental crust in Nares Strait, the seabed was progressively brought closer to the stronger subsurface currents. The isostatic rebound in Kane Basin has been estimated to be between 80 and 120 m (England, 1999 and references therein) which would have had considerable consequences on bottom water velocities. Our record of low sand content could possibly be related the Neoglacial cooling, beginning at *ca*. 7.8 cal. ka BP, in agreement with the general trend towards more polar conditions in the CAA from the Mid-Holocene onwards (Briner et al., 2016 and references therein; Lecavalier et al., 2017). Progressive atmospheric cooling would have promoted sea ice occurrence which can stabilise tidewater glacier margins (Reeh et al., 2001) and inhibited iceberg drifting in the strait. Although confronted to ambiguous data, Pienkowski et al. (2012) also reported overall deteriorating surface conditions in Barrow Strait after 7.8 cal. ka BP which became more evident after 6.7 cal. ka BP (ΔR=335). In the same area, Vare et al. (2009) echoes these observations of stronger seasonal sea ice after 6 cal. ka BP (ΔR=290) as evidence by IP_{25} fluxes. Increasing (but fluctuating) sea ice cover was also documented in northern Baffin Bay after 7.3 cal. ka BP (ΔR=0, Knudsen et al., 2008; Levac et al., 2001,) along with indications of higher productivity rates between ~6 and 4 cal. ka BP (ΔR=0) which have been linked to the inception of the North Water Polynya (Knudsen et al., 2008, Levac et al., 2001; Mudie et al., 2004). The prevailing cold conditions in the CAA which may have favoured the occurrence of sea ice in Kane Basin, combined with the shoaling of the Nares Strait region were most likely determinant in the establishment of the polynya in northern Baffin Bay after *ca*. 6 cal. ka BP through the formation of ice arches in Smith

Sound and favourable oceanographic circulation induced by the change in water depth. Interestingly, increased sedimentation rates in Kane Basin between ~4.5 and 2.8 cal. ka BP (Fig.3) coincide with a period of atmospheric warming recorded in the Agassiz ice core (Lecavalier et al., 2017). These higher sedimentation rates may have been associated with increased delivery of sediment by meltwater from the GIS and the residual ice caps on Ellesmere Island during a warmer period. The increase in the contribution of the coarse fraction in core AMD14-Kane2B over the last 1.9 cal. ka BP is suggestive of minimal seasonal sea ice and/or higher calving rates over the last two millennia in Kane Basin. This broadly coincides with low absolute diatom abundances in northernmost Baffin Bay, attesting to poor productivity rates after 2.7 cal ka BP, $\Delta R=0$ (Knudsen et al., 2008). The "bridge dipole" between Kane Basin and northernmost Baffin Bay entails that when sea-ice conditions in Kane Basin are strong, surface conditions to the south of Smith Sound are largely open and the NOW Polynya is productive, and *vice versa* (Barber et al., 2001). This inverse relationship between sea-ice conditions in Kane Basin and northernmost Baffin Bay has probably been accurate for the past *ca*. 6 cal. ka BP. Recent instabilities in the ice arch in Kane Basin that have led to increased sea-ice export towards northernmost Baffin Bay have been observed by satellite imagery and hence are only documented for the past few decades. Together with Knudsen's et al. (2008) study in northern Baffin Bay, our results suggest that these instabilities may have begun as early as *ca*. 1.9 cal. ka BP. Late Holocene decreases in sea-ice occurrence, indicative of milder conditions, were also documented in other sectors of the CAA such as in Barrow Strait between 2.0 and 1.5 cal. ka BP (Pienkowski et al., 2012) or in the adjacent Lancaster Sound between 1.2 and 0.8 cal. ka BP (Vare et al., 2009).

5 Conclusion

Our investigation of core AMD14-Kane2b has provided, for the first time, a paleo-environmental reconstruction in Kane Basin over the last *ca*. 9.0 cal. ka. Our findings concerning the successive paleo-environments in this central sector of Nares Strait following ice sheet retreat can be summarised as followed.

While evolving from a short-lived ice-proximal depositional environment at ~9.0 cal. ka BP to a rather secluded and narrow bay as the ice sheets retreated, compelling evidence indicates that Kane Basin was not connected to Hall Basin until the collapse of the GIS/IIS saddle in Kennedy Channel at ~8.3 cal. ka BP. Sea-ice cover in Kane Basin was likely moderate before the opening of Kennedy Channel, owing to high atmospheric temperatures (Lecavalier et al., 2017), but occurring nonetheless at these high latitudes due to proglacial cooling induced by the nearby GIS and IIS. The collapse of the glacial buttress in Kennedy Channel triggered the acceleration of glacial fluxes toward Nares Strait, increasing calving and iceberg-rafted debris in Kane Basin between 8.3 and 7.5 cal. ka BP. Instabilities in the GIS eventually resulted in the rapid retreat of glacial ice from eastern Kane Basin at 8.1 cal. ka BP. As the basin underwent shoaling induced by the glacio-isostatic rebound, seasonal sea ice increased significantly after 7.5 cal. ka BP with Neoglacial cooling. This stability in sea-ice occurrence was likely responsible for the inception of the NOW Polynya. A deterioration in sea-ice conditions and/or increased iceberg release appear to have taken place over the last 1.9 cal. ka BP.

This archive provides a new viewpoint that has enabled us to propose a continuous timeline of the events related to the deglaciation of Nares Strait, which until now relied entirely on land-based studies. Our study suggests that the "bridge dipole" presented in Barber et al. (2001) where warmer (colder) years exhibit more (less) sea ice in Smith Sound and less (more) ice in Nares Strait, can be extrapolated over the last *ca*. 6 cal. ka BP. High productivity rates in the NOW Polynya are however also fuelled by the throughflow of nutrient-rich Pacific water via Nares Strait and further investigation into how oceanographic circulation responded to postglacial changes in Nares Strait will provide more insight into the Holocene evolution of this highly productive area of the Arctic. Other than emphasising the need for further research into local reservoir age corrections, our study is inclined to contribute to future work on the export of low salinity Arctic water and Holocene variations of deep water formation (Hoogaker et al., 2014; Moffa-Sanchez and Hall, 2017).

Acknowledgments

E. Georgiadis' studentship is funded by both the Initiative d'Excellence (IdEx) programme of the University of Bordeaux and the Natural Science and Engineering Research Council of Canada (NSERC). We would like to thank Sofia Ribeiro, Audrey Limoges and Karen Luise Knudsen for constructive conversations on the history of North Water Polynya and Benoit Lecavalier for having shared with us the much appreciated Agassiz ice core temperature record. This work is supported by the Fondation Total, the French Agence Nationale de la Recherche (GreenEdge project), the Network of Centres of Excellence ArcticNet and the European Research Council (StG IceProxy). Finally, we wish to thank the CCGS *Amundsen* captain, officers and crew for their support during the 2014 ArcticNet cruise.

References

Andrews, J., T., and Ives, J. D.: "Cockburn" Nomenclature and the Late Quaternary History of the Eastern Canadian Arctic, Arctic and Alpine Research, 10:3, 617-633, 1978.

Albertson, M.L., Dai, Y.B., Jensen, R.A. Rouse, H.: Diffusion of submerged jets. Transactions of the American Society of Civil Engineers 115, 639-664, 1950

Axford, Y., Briner, J. P., Miller, G. H., Francis, D. R.: Paleoecological evidence for abrupt cold reversals during peak Holocene warmth on Baffin Island, Arctic Canada. QUATERNARY SCI. REV. 71, 142-149, 2009.

Bailey, W. B.: Oceanographic Features of the Canadian Archipelago, J. of the Fisheries Research Board of Canada, 14, 5, 1957.

Barber, D.G., Hanesiak, J. M., Chan, W., Piwowar, J.: Sea-ice and meteorological conditions in Northern Baffin Bay and the North Water polynya between 1979 and 1996, Atmos.-Ocean, 39:3, 343-359, 2001.

Bahr, A., F. J. Jimenez-Espejo, N. Kolasinac, P. Grunert, F. J. Hern_andez-Molina, U. Rohl, A. H. L. Voelker, C. Escutia,D. A. V. Stow, D. Hodell, and C. A. Alvarez-Zarikian.: Deciphering bottom current velocity and paleoclimate signals from contourite deposits in the Gulf of C_adiz during the last 140 kyr: An inorganic geochemical approach, Geochem. Geophys. Geosyst., 15, 3145–3160, doi:10.1002/2014GC005356, 2014.

Belkin, I. M., Levitus, S. Antonov, J. Malmberg, S.A:. "Great Salinity Anomalies" in the North Atlantic. Prog. Oceanogr. 41, 1–68, 1998.

Bennike, O., Dawes, P. R., Funder, S., Kelly, M. Weidick, A.: The late Quaternary history of Hall Land, Northwest Greenland: Discussion. Can. J. Earth Sci. 24, 370–374, 1987.

Bennike, O.: Late Quaternary history of Washington Land, North Greenland. Boreas 31, 260–272, 2002.

Blaauw, M.: Methods and code for 'classical' age-modelling of radiocarbon sequences. Quat. Geochronol. 5, 512-518, 2010.

Blake, W. Jr.: Age determination on marine and terrestrial materials of Holocene age, southern Ellesmere Island, Arctic Archipelago. Geol. Surv. Can. 79-1C, 105–109, 1979.

Blake, W., Jr., Boucherle, M. M., Fredskild, B., Jannssens, J. A., Smol, J. P.: The geomorphological setting, glacial history and Holocene development of 'Kap Inglefield Sø', Inglefield Land, North-West Greenland. Meddelelser om Grønland, Geosci. 27, 1992.

Blake, W. Jr., Jackson, H. R. Currie, C. G.: Seafloor evidence for glaciation, northernmost Baffin Bay. B. Geol. Soc. Den. 43, 157–168, 1996.

Bradley, R.S.: Holocene paleoclimatology of the Queen Elizabeth islands, Canadian high arctic. QRS. 9 (4), 365-384. http://dx.doi.org/10.1016/0277-3791(90)90028-9, 1990.

Briner, J.P., Nicholas P. McKay, N.P., Axford, Y., Bennike, O., Bradley, R. S., de Vernal, A., Fisher, D., Francus, P., Fréchette, B., Gajewski, K., Jennings, A., Kaufman, D. A., Miller, G., Rouston, C., Wagner, B.: Holocene climate change in Arctic Canada and Greenland, Quaternary Sci. Rev., 1-25, 2016.

Christie, R. L.: Geological reconnaissance of northeastern Ellesmere Island, district of Franklin. Geol. Surv. Can., Memoir 331, 1964.

Christie, R. L.: Northeastern Ellesmere Island: Lake Hazen region and Judge Daly Promontory structural geology, stratigraphy and palaeontology. Geol. Surv. Can. Report of Activities 74-1 (A). 105, 297-299, 1973.

Coulthard, R.D., Furze, M. F. A., Pienkowski, A. J., Nixon, F. C., England, J. H.: New marine DR values for Arctic Canada. Quat. Geochronol. 5, 419–434, http://dx.doi.org/10.1016/j.quageo.2010.03.002, 2010.

Oakey, G. N. and Damaske, D.: Continuity of basement structures and dyke swarms in the Kane Basin region of central Nares Strait constrained by aeromagnetic data. Polarforschung 74 (1), 51-62, 2004.

Davies, H. C., Dobson, M. R, Whittington, R. J.: A revised seismic stratigraphy for Quaternary deposits on the inner continental shelf of Scotland between 55]30'N and 57°30'N. Boreas, 13, 49-66, 1984.

Dawes, P. R.: Precambrian to Tertiary of northern Greenland, in Escher, A., and Watt, W.S., eds.), Geology of Greenland. Geol. Surv. Greenland, 248-303, 1976.

Dawes, P. R., and Garde, A. A.: Geological map of Greenland, 1:500,000, Humboldt Gletscher, sheet 6. Copenhagen: Geol. Surv. Den. And Greenland, 2004.

Dowdeswell, J. A., Whittington, R. J., Jennings, A. E., Andrews, J. T., Mackensen, A. & Marienfeld, P.: An origin for laminated glacimarine sediments through sea-ice build-up and suppressed iceberg rafting. Sedimentology 47, 557–576, 2000.

Dowdeswell, J. A., Elverhøi, A. Spielhagen, R.: Glacimarine sedimentary processes and facies on the polar north Atlantic margins. QRS 17, 243-272, 1998.

Dowdeswell, J. A., Uenzelmann-Neben, G., Whittington, R. J., Marienfeld, P.: The Late Quaternary sedimentary record in Scoresby Sund, East Greenland. Boreas 23, 294–310, 1994.

Dyke, A. S., Hooper, J. M. G., Savelle, J. M.: A history of sea ice in the Canadian Arctic Archipelago based on postglacial remains of the bowhead whale (Balaena mysticetus). Arctic 49, 235–255, 1996a.

Dyke, A. S., Andrews, J. T., Clark, P. U., England, J. H., Miller, G. H., Shaw, J., & Veillette, J. J.: The Laurentide and Innuitian ice sheets during the last glacial maximum. QuaternarySci. Rev., 21 (1), 9-31, 2002.

Elverhøi. A.. Liestel. O., Nagy. J.: Glacial erosion, sedimentation and microfauna in the inner part of Kongsfjor- den. Spitsbergen. Norsk Polarinrtitutt Skrifter 172. 33- 58, 1980.

England, J. HK, Lakeman, T. R., Lemmen, D. S., Bednarski, J. M., Stewart, T. G., Evans, D. J. A.: A millennial-scale record of Arctic Ocean sea ice variability and the demise of the Ellesmere Island ice shelves. Geoph. Res. Lett. 35, doi:10.1029/2008GL034470, 2008.

England, J., Dyke, A. S., Coulthard, R. D., McNeely, R. & Aitken, A.: The exaggerated radiocarbon age of deposit-feeding molluscs in calcareous environments. Boreas, 42, 362–373. 10.1111/j.1502- 3885.2012.00256.x. ISSN 0300-9483, 2013.

England, J.: Coalescent Greenland and Innuitian ice during the Last Glacial Maximum: Revising the Quaternary of the Canadian High Arctic. Quaternary Sci. Rev. 18:421–426, http://dx.doi.org/10.1016/ S0277-3791(98)00070-5, 1999.

Fisher, D., Zheng, J., Burgess, D., Zdanowicz, C., Kinnard, C., Sharp, M., Bourgeois, J.: Recent melt rates of Canadian Arctic ice caps are the highest in four millennia, Global and Planet. Change, 84-85, 3-7, doi: 10.1016/j.gloplacha.2011.06.005, 2011.

Funder, S., Goosse, H., Jepsen, H., Kaas, E., Kjær, K. H., Korsgaard, N. J.,. Larsen, N. K., Linderson, H., Lyså, A., Möller, P., Olsen,, J., Willerslev, E.: A 10,000-Year Record of Arctic Ocean Sea-Ice Variability—View from the Beach. Science 333, 747-750, 2011.

Funder, S.: Late Quaternary stratigraphy and glaciology in the Thule area, Northwest Greenland. Meddelelser om Grønland, Geosci. 22, 1–63, 1990.

Ganeshram, R.S., Calvert, S.E., Pedersen, T.F., and Cowie, G.L.: Factors controlling the burial of organic carbon in laminated and bioturbated sediments off NW Mexico: Implications for hydrocarbon preservation, Geochim. Cosmochim. Acta, 63 (11–12), 1723–1734, doi:10.1016/S0016-7037(99)00073-3, 1999.

Gilbert, R.: Sedimentary processes of Canadian Arctic fjords. Sedimentary Geology 36, 147-175, 1983.

Harrison, J. C., St-Onge, M.R., Petrov, O.V., Strelnikov, S. I., Lopatin, B. G., Wilson, F. H., Tella, S., Paul, D., Lynds, T., Shokalsky, A. P., Hults, C. K., Bergman, S., Jepsen, H. F., Solli, A.: Geological map of the Arctic. Geol. Surv. Can., Map 2159A, scale 1:5 000 000, 2011.

Harrison, J. C., Brent, T. A., and Oakey, G. N.: Bedrock Geology of the Nares Strait Region of Arctic Canada and Greenland, with explanatory text and GIS content. Geol. Surv. Can., Open File 5278, 74 (1-3), 185-189, 2006.

Hein, F. J. and Syvitski, J. P. M.: Sedimentary environments and facies in an Arctic basin, Itirbilung Fiord, Baffin Island, Canada. Sediment. Geol., 81: 17-45, 1992.

Hogan, K., Ó Cofaigh, C., Jennings, A., Dowdeswell, J., Hiemstra, J.: Deglaciation of a major palaeo-ice stream in Disko Trough, West Greenland. Quaternary Sci. Rev., 147, 5-26, 2016.

Hoogakker, B. A. A., McCave, I. N., Elderfield, H., Hillaire-Marcel, C., Simstich, J.: Holocene climate variability in the Labrador Sea. J. Geol. Soc. London 172, 272-277. doi.org/10.1144/jgs2013-097, 2014.

Jakobsson, M., Hogan, K. A., Mayer, L. A., Mix, A., Jennings, J., Stoner, J., Eriksson, B., Jerram, K., Mohammad, R., Pearce, C., Reilly, B., Stranne, C., 2018: The Holocene retreat dynamics and stability of Petermann Glacier in northwest Greenland. Nat. Commun. 9, doi.org/10.1038/s41467-018-04573-2, 2104.

Jennings, A. E., Sheldon, C., Cronin, T. M., Francus, P., Stoner, J. Andrews, J. T.: The Holocene history of Nares Strait: transition from glacial bay to Arctic-Atlantic throughflow. Oceanography 24, 26–41, 2011.

Jones, E. P., Swift, J.H., Anderson, L. G., Lipizer, M., Civitarese, G., Falkner, K. K., Kattner, G., McLaughlin, F.: Tracing Pacific water in the North Atlantic Ocean, J. Geophys. Res., 108 (C4), 3116, doi:10.1029/2001JC001141, 2003.

Jones, E. P., Eert, A. J., (printed 2006). Waters of Nares Strait in 2001. Polarforschung 74 (1-3), 185-189, 2004.

Kalkreuth, W. D., McCullough, K. M., Richardson, R. J. H.: Geological, Archaeological, and Historical Occurrences of Coal, East-central Ellesmere Island, Arctic Canada. Arctic Alpine Res. 25 (4), 277-307, 1993.

Kelly, M. and Bennike, O.: Quaternary Geology of Western and Central North Greenland. Rapport Grønlands Geologiske Undersøgelse 153, 34, 1992.

Kelly, M., Funder, S., Houmark-Nielsen, M., Knudsen, K. L., Kronborg, C., Landvik, J. & Sorby, L.: Quaternary glacial and marine environmental history of Northwest Greenland: a review and reappraisal. Quaternary Sci. Rev. 18, 373–392, 1999.

Kerr, J. W.: Stratigraphy of Central and Eastern Ellesmere Island, Arctic Canada, Part I, Proterozoic and Cambrian; Geol. Surv. Can. 67-27, Part I, 1967.

Kerr, J. W.: Stratigraphy of Central and Eastern Ellesmere Island, Arctic Canada, Part II, Ordovician; Geol. Surv. Can. 67-27, Part II, 1968.

Kliem, N., Greenberg, D. A.,: Diagnostic simulations of the summer circulation in the Canadian Arctic Archipelago, Atmos.-Ocean 41:4, 273-289, DOI: 10.3137/ao.410402, 2003.

Koch, L.: Stratigraphy of Greenland. Meddr. Grønland 73 (2), 205-320, 1929a..

Koch, L.: The Geology of the South Coast of Washington Land. Meddr. Grønland 73, (2), 205-320, 1929b.

Koch, L.: The geology of Inglefield Land. Meddr. Grønland 73 (2), 38, 1933.

Knudsen, K. L., Stabell, B., Seidenkrantz, M.-S., Eirıksson, J., Blake, W., Jr.: Deglacial and Holocene conditions in northernmost Baffin Bay: sediments, foraminifera, diatoms and stable isotopes. Boreas 37, 346–376. 10.1111/j.1502-3885.2008.00035.x. ISSN 0300-9483, 2008.

Kravitz, J.H.: Textural and Mineralogical Characteristics of the Surficial Sediments of Kane Basin. J. Sedimetary Petrology. 46 (3), 710-725, 1976.

Kravitz, J. H.: Sediments and sediment processes in Kane Basin, a high Arctic glacial marine basin. University of Colorado, Institute of Arctic Alpine Res. Occasional Paper 39, 1982.

Lecavalier, B. S., Fisher, D. A., Milne, G. A., Vinther, B. M., Tarasov, L., Huybrechts, P., Lacelle, D., Main, B., Zheng, J., Bourgeois, J., Dyke, A .S.: High Arctic Holocene temperature record from the Agassiz ice cap and Greenland ice sheet evolution. PNAS 114 (23), 5952-5957. doi: 10.1073/pnas.1616287114, 2017.

Levac, E., de Vernal, A., Blake, W. Jr.: Sea-surface conditions in the northernmost Baffin Bay during the Holocene: Palynological evidence. J. Quaternary Sci. 16, 353–363, 2001.

List, E.J.: Turbulent jets and plumes. Annu. Rev. Fluid Mech. 14, 189-212, 1982.

MacGregor, J. A., Colgan, W. T., Rahnestock, M. A., Morlighem, M., Catania, G. A., Paden, G. A., Gogineni, S. P.: Holocene deceleration of the Greenland Ice Sheet. Science 351, 6273, 590-593. DOI: 10.1126/science.aab1702, 2016.

McGeehan, T., and W. Maslowski,: Evaluation and control mechanisms of volume and freshwater export through the Canadian Arctic Archipelago in a high-resolution pan-Arctic ice ocean model. J. Geophys. Res., 117, C00D14, doi:10.1029/ 2011JC007261, 2012.

McNeely, R., Dyke, A. S., Southon, J. R.: Marine Reservoir Ages Preliminary Data Assessment. Geol. Surv. Can. Open File 5049, 2006.

Melling, H., Gratton, Y., Ingram, R. G.: Ocean circulation within the North Water polynya of Baffin Bay. Atmos.-Ocean 9 (3), 301–325. doi:10.1080/07055900.2001.9649683, 2001.

Miall, A. D.: Tertiary sedimentation and tectonics in the Judge Daly Basin, northeast Ellesmere Island, Arctic Canada. Geol. Surv. Can. 80-30, 1982.

Moffa-Sanchez, P. and Hall, I. R.: North Atlantic variability and its links to European climate over the last 3000 years. Nat. Commun., 1726, 2017.

Moynihan, M. J.: Oceanographic observations in Kane Basin, September 1968 and July–September 1969. United States Coast Guard Oceanographic Report 55, 70, 1972.

Mudie, P. T., Rochon, A., Prins, M. A., Soenarjo, D., Troelstra, S. R., Levac, E., Scott, D. B., Roncaglia, L., Kuijpers, A., (printed 2006): Late Pleistocene–Holocene marine geology of Nares Strait region: Palaeoceanography from foraminifera and dinoflagellate cysts, sedimentology and stable isotopes. Polarforschung 74, 169–183, 2004.

Muench, R. D.: Oceanographic conditions at a fixed location in western Kane Basin, May 1969, Oceanogr. Rep. CG 373-44, 1-5, U.S. Coast Guard, Washington, D.C, 1971.

Mulder, T., Hassan, R., Ducassou, E., Zaragosi, S., Gonthier, E., Hanquiez, V., Marchès, E., Toucanne, S.: Contourites in the Gulf of Càdiz: A cautionary note on potentially ambiguous indicators of bottom current velocity, Geo.Mar. Lett., 33(5), 357–367, doi:10.1007/s00367-013-0332-4, 2013.

Münchow, A.: Volume and freshwater flux observations from Nares Strait to the west of Greenland at daily time scales from 2003 to 2009. J.Phys. Oceanogr., 46 (1), 141–157. doi: 10.1175/JPO-D-15-0093.1, 2016.

Münchow, A., Falkner, K. K. Melling, H.: Spatial continuity of measured seawater and tracer fluxes through Nares Strait, a dynamically wide channel bordering the Canadian Archipelago. J. Mar. Res., 65, 759–788, doi:10.1357/002224007784219048, 2007.

Münchow, A., Melling, H., Falkner, K. K.: An observational estimate of volume and freshwater flux leaving the Arctic Ocean through Nares Strait. J. Phys. Oceanogr., 36, 2025–2041, 2006.

Mundy, C.J. and Barber, D.G.: On the relationship between spatial patterns of sea-ice type and the mechanisms which create and maintain the North Water (NOW) polynya, Atmos.-Ocean 39 (3), 327-341, DOI: 10.1080/07055900.2001.9649684, 2001.

Nürnberg, D., Wollenburg, I., Dethleff, D., Eicken, H., Kassens, H., Letzig, T., Reimnitz, E., Thiede, J.: Sediments in Arctic sea ice: implications for entrainment, transport and release. Mar. Geol., 119, 185-214, 1994.

Ó Cofaigh, C. and Dowdeswell, J. A.: Laminated sediments in glacimarine environments: diagnostic criteria for their interpretation. Quaternary Sci. Rev. 20, 1411–1436, 2001.

Ó Cofaigh, C., Dowdeswell, J. A., Grobe, H.: Holocene glacimarine sedimentation, inner Scoresby Sund, East Greenland: the influence of fast-flowing ice-sheet outlet glaciers. Mar. Geol. 175, 103–129, 2001.

Osterman, L.E. and Andrews, J.T.: Changes in glacial-marine sedimentation in core HU77-159, Frobisher Bay, Baffin Island, N.W.T.: a record of proximal, distal, and ice-rafting glacial-marine environments; in Glacial-Marine Sedimentation, B.F. Molnia (ed.), Plenum Press, New York, 451–493, 1983.

Pedersen, T. F., Shimmield, G. B., Price, N. B.: Lack of enhanced preservation of organic matter in sediments under the oxygen minimum on the Oman margin, Geochim. Cosmochim. Acta, 56 (1), 545–551, doi:10.1016/0016-7037(92)90152-9, 1992.

Pfirman, S., Wollenburg, I., Thiede, J., Lange, M.A.: Lithogenic sediment on Artic pack ice: potential aeolian flux and contributions to deep sea sediments. In: Paleoclimatology and Paleometeorology: Modern and Past Pattern of Global Atmospheric Transport. Sarnthein, M., Leinen, M. (Eds.), Kluwer, Dordrecht, 463–493, 1989.

Pienkowski, A. J., England, J. H., Furze, M. F. A., Marret, F., Eynaud, F., Vilks, G., MacLean B., Blasco, S., Scourse, J. D.: The deglacial to postglacial marine environments of SE Barrow Strait, Canadian Arctic Archipelago. Boreas 41, 141–179. 10.1111/j.1502-3885.2011.00227.x. ISSN 0300-9483, 2012.

Rabe, B., Johnson, H. L., Münchow, A. Melling, H.: Geostrophic ocean currents and freshwater fluxes across the Canadian polar shelf via Nares Strait. J. Mar. Res. 70, 603–640, 2012.

Reeh, N., Thomsen, H. H., Higgins, A. K., Weidick, A.: Sea ice and the stability of north and northeast Greenland floating glaciers. Ann. Glaciol. 33, 474-480, 2001.

Reimer, P. J., Bayliss, E. B. A., Beck, J. W., Blackwell, P. G., Ramsey, C. B., Buck, C. E., Cheng, H., Edwards, R. L., Friedrich, M., Grootes, P. M., Guilderson, T. P., Haflidason, H., Hajdas, I., Hatté, C., Heaton, T. J., Hoffmann, D. L., Hogg, A. G., Hughen, K. A., Kaiser, K. F., Kromer, B., Manning, S. W., Niu, M., Reimer, R. W., Richards, D. A., Scott, A. M., Southon, J. R., Staff, R. A., Turney, C. S. M., van der Plicht, J.: IntCal13 and MARINE13 radiocarbon age calibration curves 0-50,000 years cal. BP. Radiocarbon 55 (4), 1869–1887, 2013.

Samelson, R. M., Barbour, P. L.: Low-level winds in Nares Strait: A model-based mesoscale climatology. Mon. Weather Rev., 136, 4746–4759, 2008.

Stuiver, M., Reimer, P.J., Reimer, R.W.: CALIB 7.1 [WWW program] at http://calib.org, 2018.

Svendsen, J.I., Mangerud, J., Elverhøi, A., Solheim, A. and Schüttenhelm, R. T. E.: The Late Weichselian glacial maximum on western Spitsbergen inferred from offshore sediment cores. Mar. Geol., 104, 1-17, 1992.

Tjallingii, R., Röhl, U., Kölling, M., Bickert, T.: Influence of the water content on X-ray fluorescence core-scanning measurements in soft marine sediments, Geochem. Geophys. Geosyst. 8, Q02004, doi:10.1029/2006GC001393, 2007.

Syvitski, J. P. M.: Towards an understanding of sediment deposition on glaciated continental shelves. Cont. Shelf Res., 11 (8-10), 897-937, 1991.

Tushingham, A. M.: On the extent and thickness of the Innuitian Ice Sheet: a postglacial-adjustment approach. Can. J. Earth Sci. 28, 2, 231-239, 1990.

Vare, L.L., Massé, G., Gregory, T.R., Smart, C.W., Belt, S.T.: Sea ice variations in the central Canadian Arctic Archipelago during the Holocene. Quaternary Sci. Rev. 28, 1354–1366, 2009.

Vinther, B. M., Clausen, H., B., Johnsen,S. J., Rasmussen, S. O., Andersen, K. K.,Buchardt, S. L., Dahl-Jensen, D., Seierstad, I. K., Siggaard-Andersen, M. L., Steffensen, J. P., Svensson, A., Olsen, J., Heinemeier, J.: A synchronized dating of three Greenland ice cores throughout the Holocene, J. Geophys. Res., 111, D13102, doi:10.1029/2005JD006921, 2006.

Zaragosi, S., Bourillet, J.-F., Eynaud, F., Toucanne, S., Denhard, B., Van Toer, A., Lanfumey, A.: The impact of the last European deglaciation on the deep-sea turbidite systems of the Celtic-Armorican margin (Bay of Biscay). Geo-Mar. Lett. 26, 317-329. DOI 10.1007/s00368-006-0048-9, 2006.

Zreda, M., England, J., Phillips, F., Elmore, D., Sharma, P.: Unblocking of the Nares Strait by Greenland and Ellesmere Ice-Sheet retreat 10,000 years ago. Nature 398:139–142, http:// dx.doi.org/10.1038/18197, 1999.

Clim. Past Discuss., https://doi.org/10.5194/cp-2018-78
Manuscript under review for journal Clim. Past
Discussion started: 11 July 2018

Climate of the Past Discussions

Table 1: AMS radiocarbon ages on selected carbonate material. Asterisks indicate data that were not used in the age model. MBF: mixed benthic foraminifera, MS: unidentified mollusc shell.

Laboratory code	Dated material	Depth (cm)	14C age (a BP)	Median probability age (cal a BP) ΔR=0	1σ ΔR=0 (cal a BP)	Median probability age (cal a BP) ΔR=240	1 σ ΔR=240 (cal a BP)
SacA-46000	MS	58.5	3150+-35	2932	2869-2984	2700	2673 - 2736
UGAMS-24304	MS	59	3125+-25	2900	2854-2941	2683	2655 - 2720
UGAMS-24305	MS	62	3010+-25*	2775	2739-2802	2502	2428 - 2575
SacA-46003	MBF	122	6125+-45*	6555	6494-6617	6205	6259 - 6356
UGAMS-24308	MS	139	3030+-25*	2793	2754-2822	2542	2469 - 2611
UCIAMS-173009	MS	139	4540+-20	4760	4764-4809	4427	4392 - 4453
UGAMS-24306	MS	152	4190+-25*	4283	4230-4339	3937	3884 - 3978
UGAMS-24307	MS	186	5445+-25	5823	5780-5876	5572	5541 - 5602
UGAMS-24295	MS	207.5	6005+-25	6417	6382-6458	6005	6168 - 6240
UCIAMS-173006	MS	238.5	8175+-20*	8651	8595-8690	8389	8363 - 8411
SacA-46002	MBF	251.5	7250+-60	7714	7649-7780	7503	7451 - 7555
SacA-45999	MBF	273.5	7870+-50	8336	8290-8388	7870	8026 - 8147
Beta-467584	MBF	297.5	7980+-30	8433	8388 - 8469	8215	8167 - 8259
UGAMS-24294	MS fragment	301.5	43700+-225*				
Beta-467583	MBF	310.5	9380+-30*	10210	10180 - 10234	9907	9821 - 10001
Beta-467583	MBF	327.5	8160+-30	8633	8577 - 8685	8379	8347 - 8405
SacA-46001	MBF	333.5	8200+-60	8709	8587-8796	8422	8358 - 8482
UCIAMS-173007	MS	358.5	8450+-20	9050	9002-9080	8703	8637 - 8752
UCIAMS-173008	MS	362.5	8520+-20	9149	9094-9205	8840	8773 - 8908
UGAMS-24296	MS	407.5	8640+-30	9318	9272-9373	8998	8968 - 9021

Clim. Past Discuss., https://doi.org/10.5194/cp-2018-78
Manuscript under review for journal Clim. Past
Discussion started: 11 July 2018

Climate of the Past Discussions
Open Access
EGU

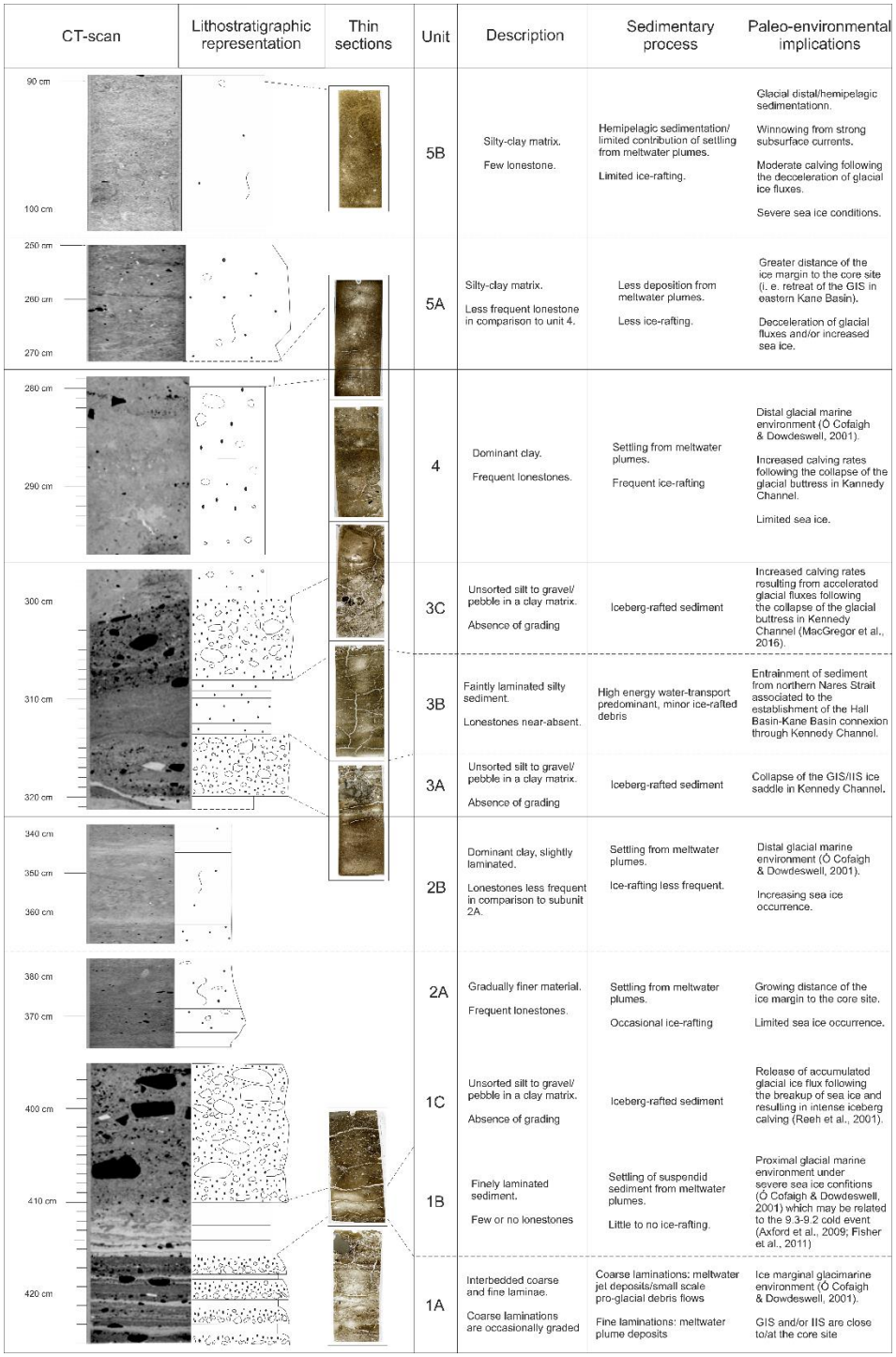

Unit	Description	Sedimentary process	Paleo-environmental implications
5B	Silty-clay matrix. Few lonestone.	Hemipelagic sedimentation/ limited contribution of settling from meltwater plumes. Limited ice-rafting.	Glacial distal/hemipelagic sedimentationn. Winnowing from strong subsurface currents. Moderate calving following the deceleration of glacial ice fluxes. Severe sea ice conditions.
5A	Silty-clay matrix. Less frequent lonestone in comparison to unit 4.	Less deposition from meltwater plumes. Less ice-rafting.	Greater distance of the ice margin to the core site (i. e. retreat of the GIS in eastern Kane Basin). Deceleration of glacial fluxes and/or increased sea ice.
4	Dominant clay. Frequent lonestones.	Settling from meltwater plumes. Frequent ice-rafting	Distal glacial marine environment (Ó Cofaigh & Dowdeswell, 2001). Increased calving rates following the collapse of the glacial buttress in Kannedy Channel. Limited sea ice.
3C	Unsorted silt to gravel/ pebble in a clay matrix. Absence of grading	Iceberg-rafted sediment	Increased calving rates resulting from accelerated glacial fluxes following the collapse of the glacial buttress in Kennedy Channel (MacGregor et al., 2016).
3B	Faintly laminated silty sediment. Lonestones near-absent.	High energy water-transport predominant, minor ice-rafted debris	Entrainment of sediment from northern Nares Strait associated to the establishment of the Hall Basin-Kane Basin connexion through Kennedy Channel.
3A	Unsorted silt to gravel/ pebble in a clay matrix. Absence of grading	Iceberg-rafted sediment	Collapse of the GIS/IIS ice saddle in Kennedy Channel.
2B	Dominant clay, slightly laminated. Lonestones less frequent in comparison to subunit 2A.	Settling from meltwater plumes. Ice-rafting less frequent.	Distal glacial marine environment (Ó Cofaigh & Dowdeswell, 2001). Increasing sea ice occurrence.
2A	Gradually finer material. Frequent lonestones.	Settling from meltwater plumes. Occasional ice-rafting	Growing distance of the ice margin to the core site. Limited sea ice occurrence.
1C	Unsorted silt to gravel/ pebble in a clay matrix. Absence of grading	Iceberg-rafted sediment	Release of accumulated glacial ice flux following the breakup of sea ice and resulting in intense iceberg calving (Reeh et al., 2001).
1B	Finely laminated sediment. Few or no lonestones	Settling of suspendid sediment from meltwater plumes. Little to no ice-rafting.	Proximal glacial marine environment under severe sea ice confitions (Ó Cofaigh & Dowdeswell, 2001) which may be related to the 9.3-9.2 cold event (Axford et al., 2009; Fisher et al., 2011)
1A	Interbedded coarse and fine laminae. Coarse laminations are occasionally graded	Coarse laminations: meltwater jet deposits/small scale pro-glacial debris flows Fine laminations: meltwater plume deposits	Ice marginal glacimarine environment (Ó Cofaigh & Dowdeswell, 2001). GIS and/or IIS are close to/at the core site

Table 2: Details of CT-scans and thin sections for each lithologic unit of core AMD14-Kane2B and summarised descriptions and interpretations. The paleo-environmental implications discussed in this study have been outlined here.

Clim. Past Discuss., https://doi.org/10.5194/cp-2018-78
Manuscript under review for journal Clim. Past
Discussion started: 11 July 2018

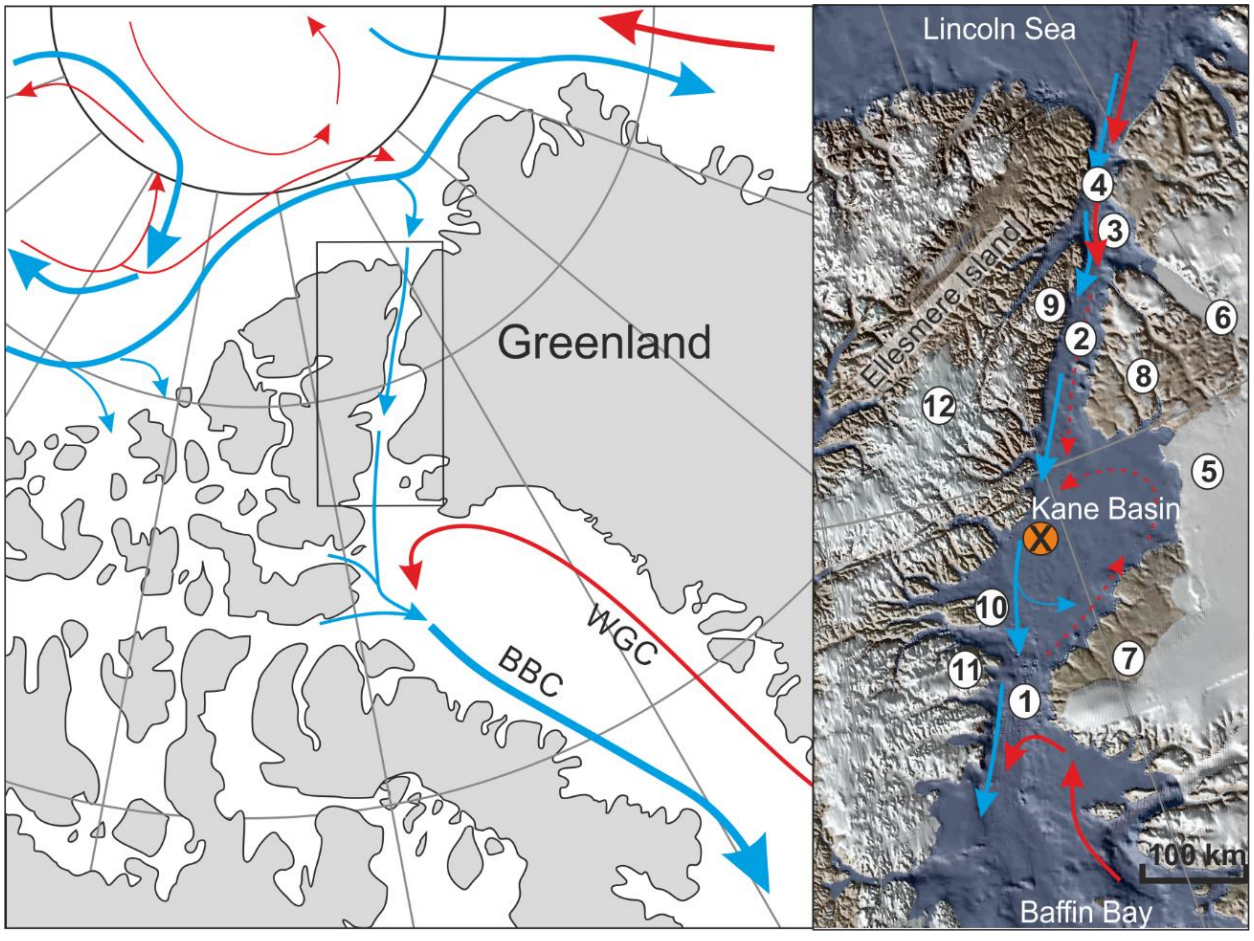

Figure 1: Schematic circulation in the Canadian and northern Greenland sectors of the Arctic Ocean (left) and within Nares Strait (right). The location of core AMD14-Kane2b is marked by a cross. Blue arrows represent Arctic water and red arrows predominantly Atlantic water. WGC: West Greenland Current, BBC: Baffin Bay Current. 1 - Smith Sound; 2 - Kennedy Channel; 3 - Hall Basin; 4 - Robeson Channel, 5 - Humboldt Glacier; 6 - Petermann Glacier; 7 - Inglefield Land; 8 - Washington Land; 9 - Judge Daly Promontory; 10 - Bache Peninsula; 11 - Johan Peninsula; 12 - Agassiz Ice Cap.

Clim. Past Discuss., https://doi.org/10.5194/cp-2018-78
Manuscript under review for journal Clim. Past
Discussion started: 11 July 2018

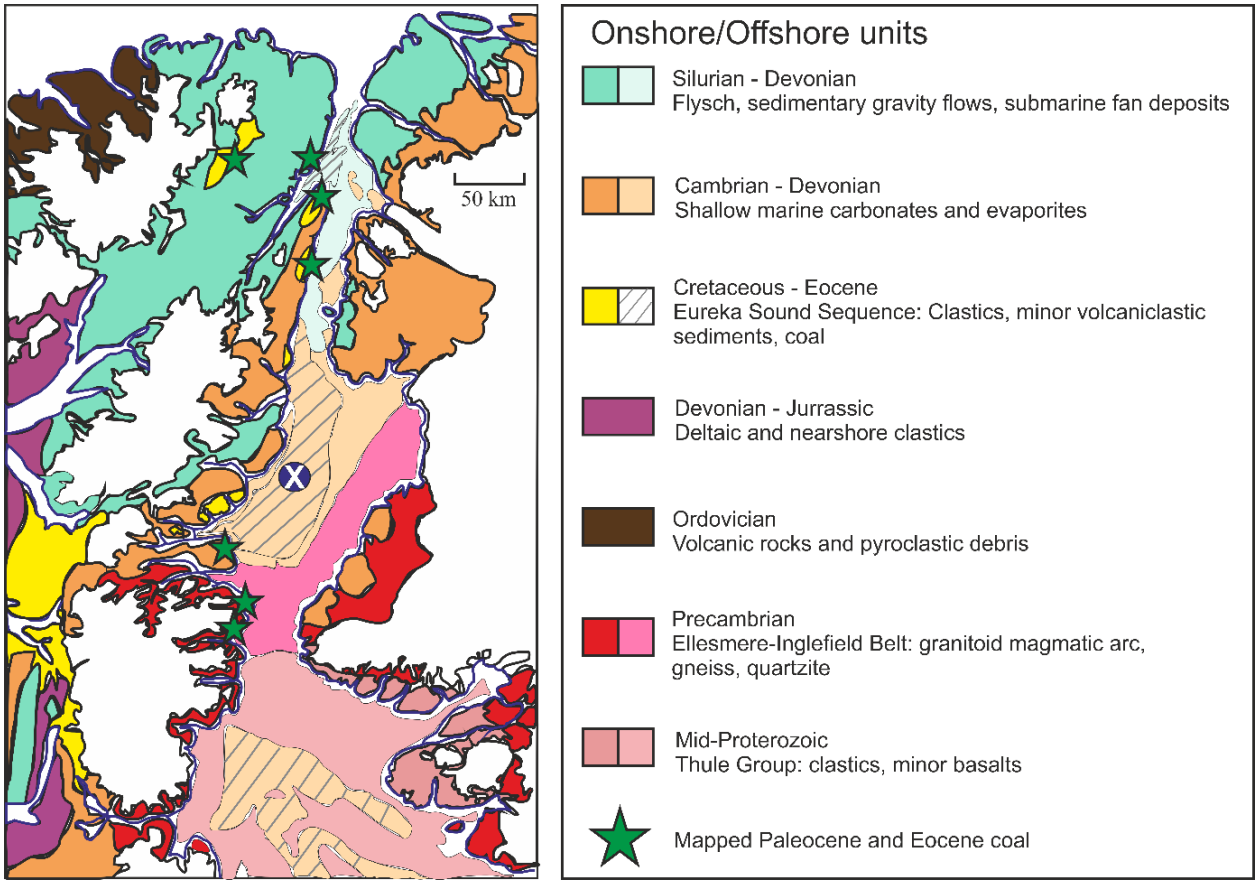

Figure 2: Geology of Northwest Greenland and Ellesmere Island along Nares Strait. Adapted from Harrison *et al.*, 2011.

Clim. Past Discuss., https://doi.org/10.5194/cp-2018-78
Manuscript under review for journal Clim. Past
Discussion started: 11 July 2018

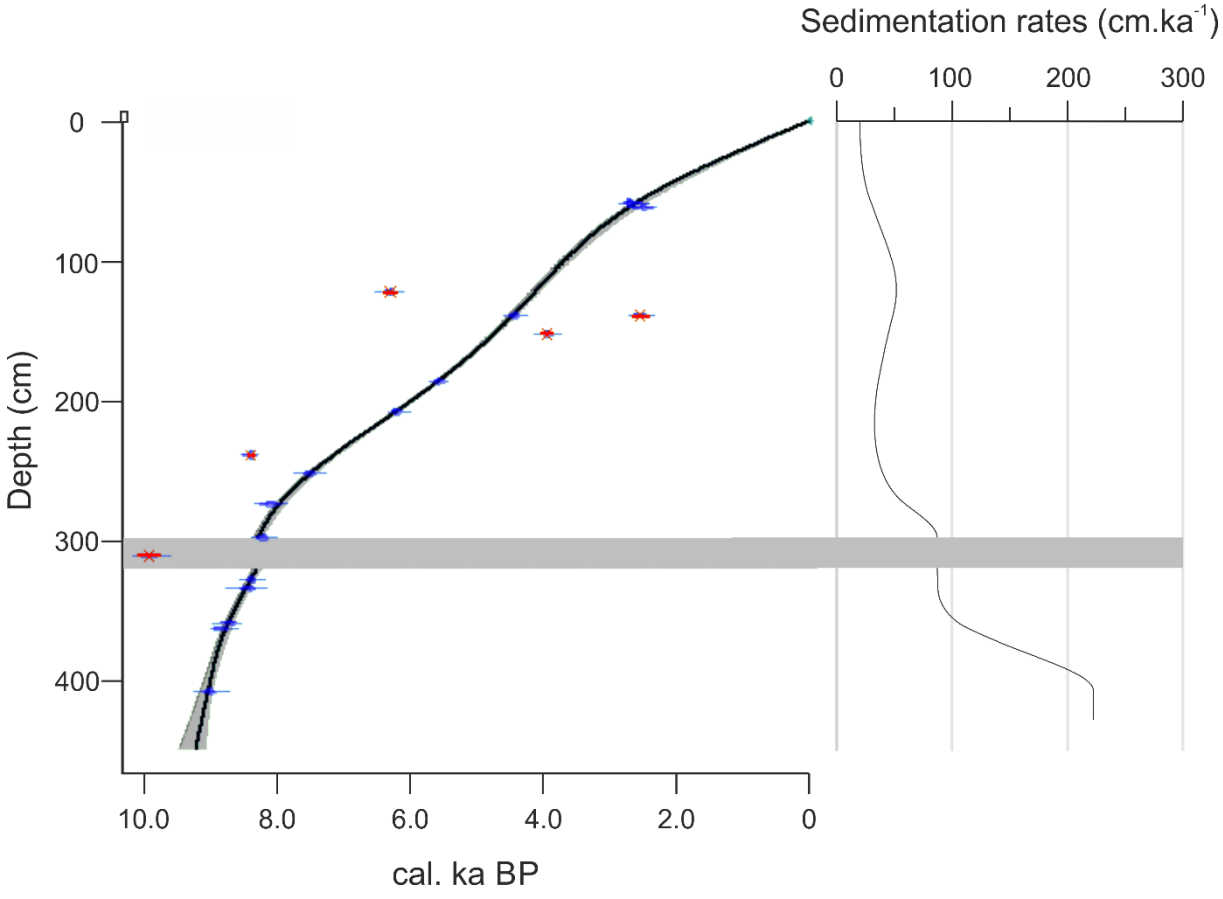

Figure 3: Core AMD14-Kane2b age model (left) and sedimentation rates (right). ^{14}C ages excluded from the age model (time reversals) are crossed out in red.

Clim. Past Discuss., https://doi.org/10.5194/cp-2018-78
Manuscript under review for journal Clim. Past
Discussion started: 11 July 2018

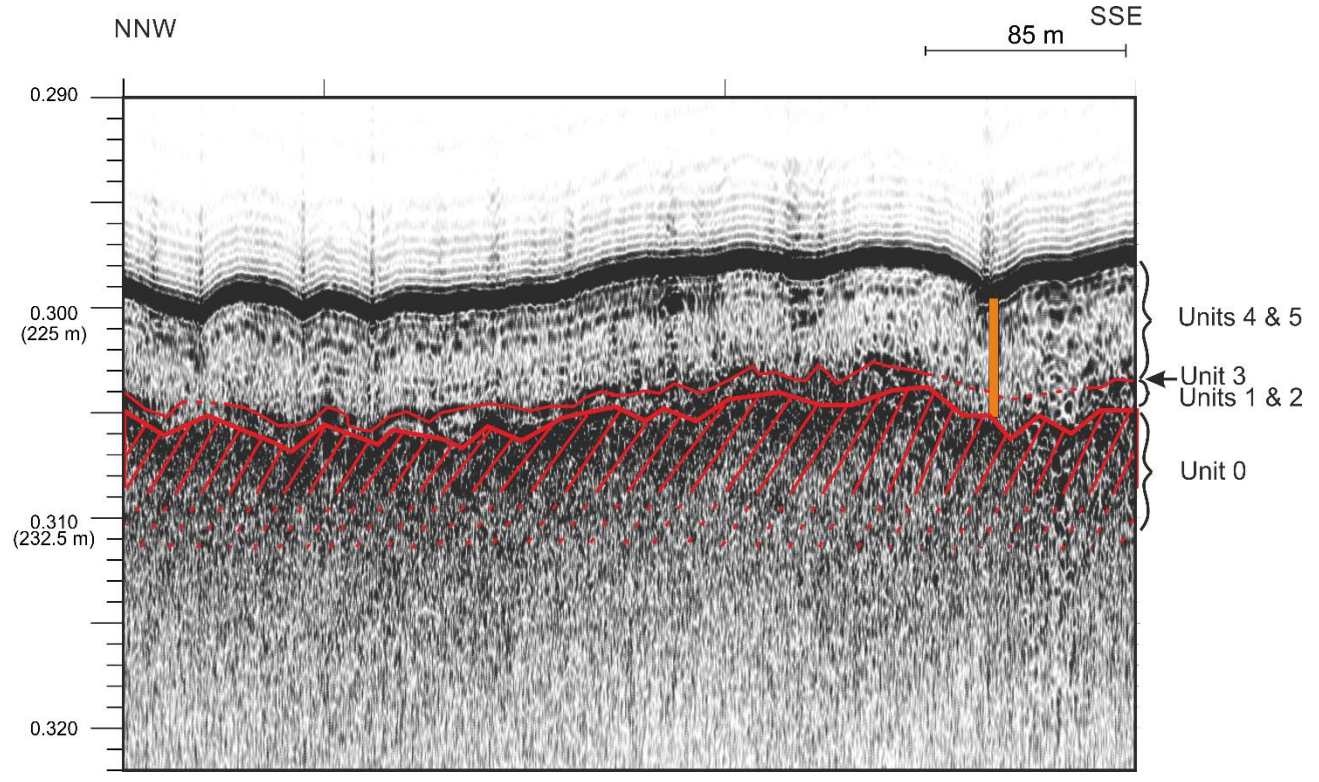

Figure 4: 3.5 kHz chirp profile across the coring location. Core AMD14-Kane2b is represented by the orange box. Vertical scale in s (TWT) with depth conversion assuming 100 ms (TWT) = 75 meters.

Clim. Past Discuss., https://doi.org/10.5194/cp-2018-78
Manuscript under review for journal Clim. Past
Discussion started: 11 July 2018

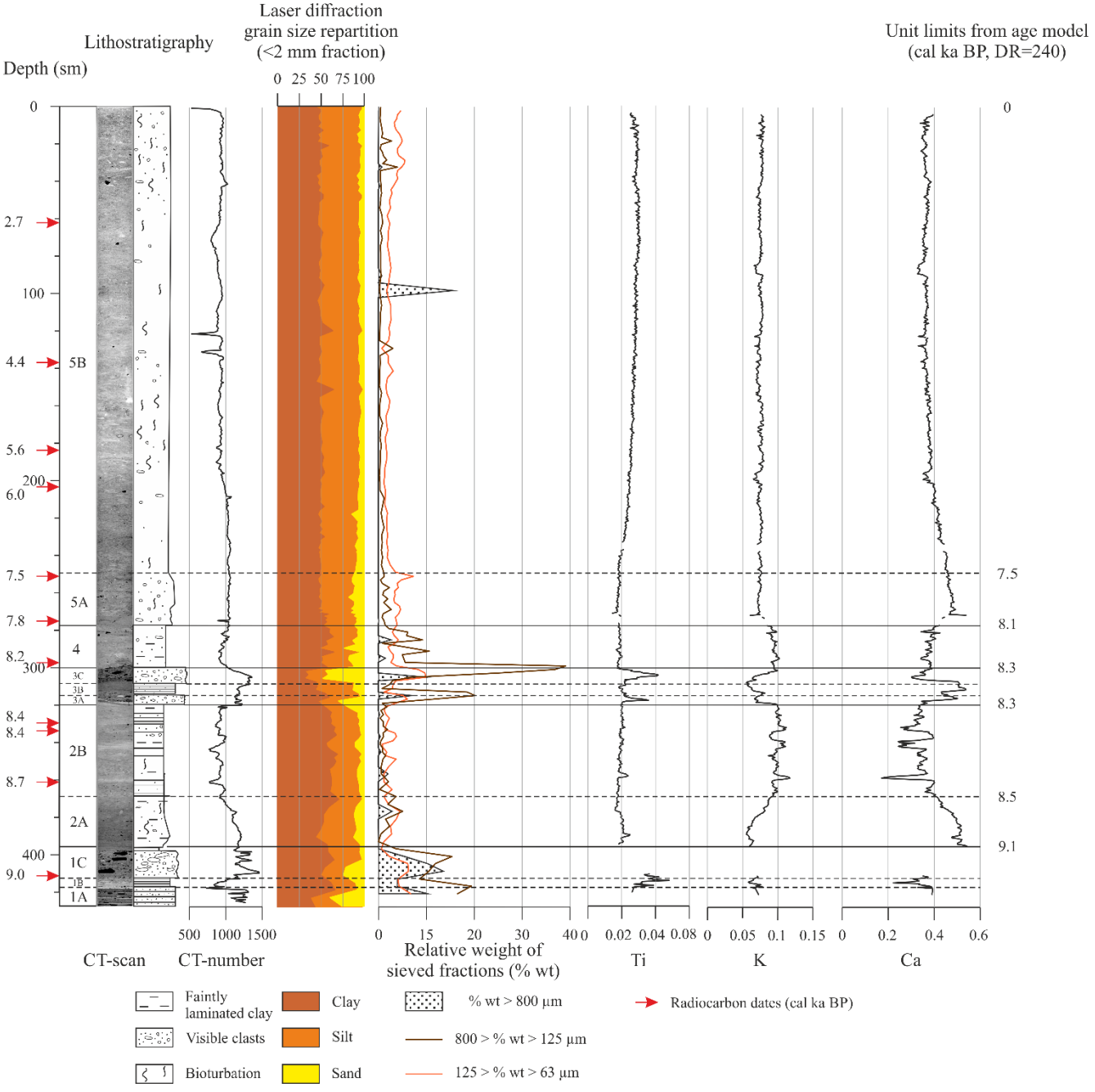

Figure 5: Sedimentological results and elemental signature of the detrital fraction of core AMD14-Kane2b. XRF-derived Ti, K, and Ca abundance were normalised to the total cps yielded by all elements (cf. Sect. 3.2). Zr counts are not shown but their profile is similar to that of Ti. Likewise, Si and Al counts vary similarly to K counts and are not shown here. XRF data were not measured in 1A and 1C due to the abundance of coarse materiel.

Clim. Past Discuss., https://doi.org/10.5194/cp-2018-78
Manuscript under review for journal Clim. Past
Discussion started: 11 July 2018

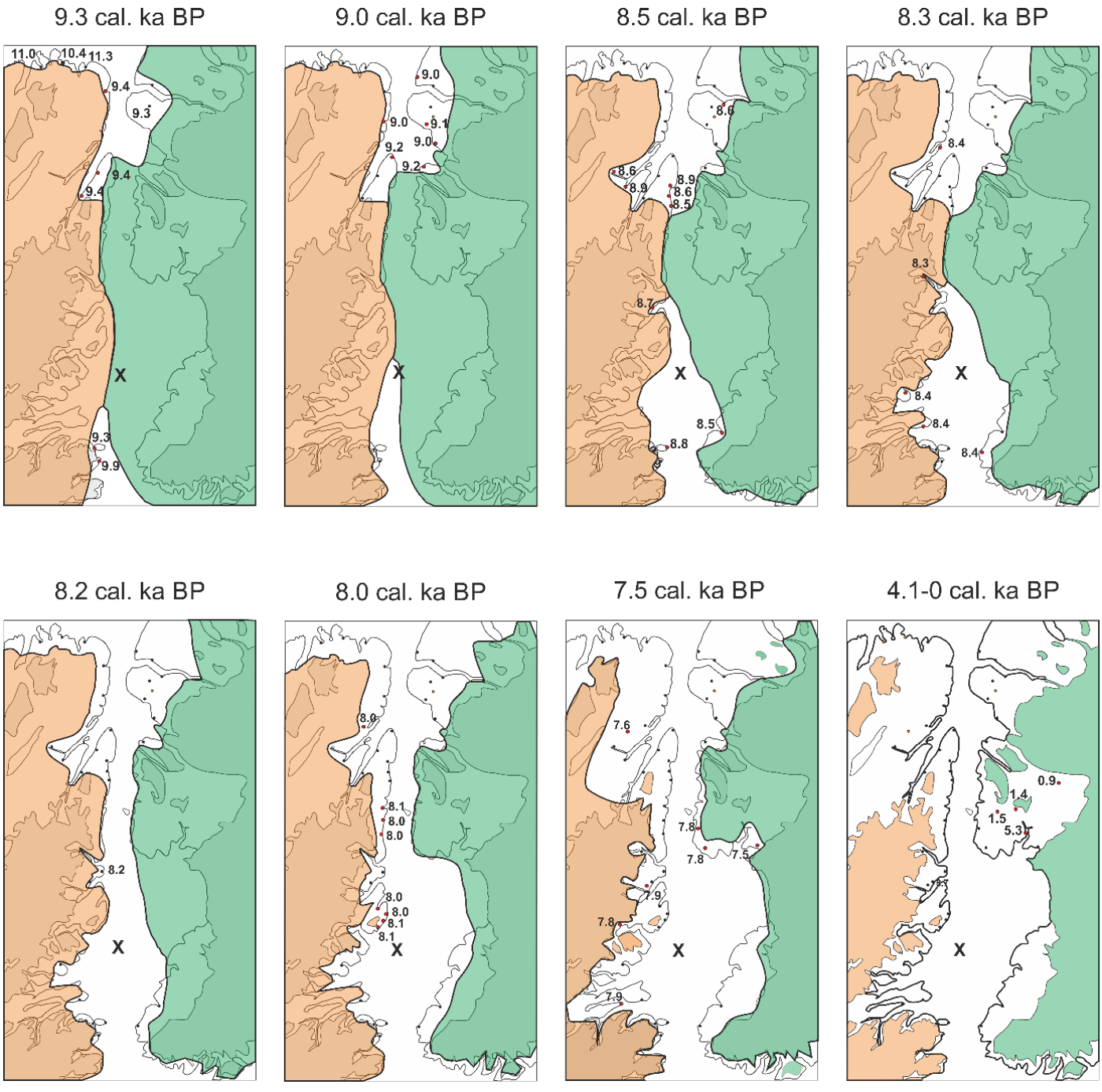

Figure 6: GIS and IIS retreat in Nares Strait. Adapted from England (1999) and includes data from Bennike (2002) for Washington Land. All mollusc ages were calibrated with ΔR= 240 using Calib 7.1. (Stuiver et al., 2018). The position of the GIS and IIS margins offshore in Kane Basin are deduced from our sedimentological and geochemical data.